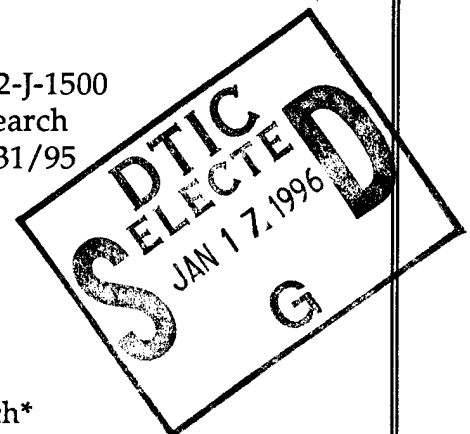# Semiannual Technical Report

Low Temperature Deposition and Characterization of N- and P-Type Silicon Carbide Thin Films and Associated Ohmic and Schottky Contacts

DTIC
SELECTED
JAN 17 1996
G

R. F. Davis and R. J. Nemanich*
M. C. Benjamin*, S. Fleming, S. Kern, and L. M. Porter
Materials Science and Engineering Department
*Department of Physics
North Carolina State University
Raleigh, NC 27695

DTIC QUALITY INSPECTED 3

December, 1995

19960111 016

REPORT DOCUMENTATION PAGE

Form Approved
OMB No. 0704-0188

1. AGENCY USE ONLY *(Leave blank)*	2. REPORT DATE	3. REPORT TYPE AND DATES COVERED
	December, 1995	Semiannual Technical 7/1/95-12/31/95

4. TITLE AND SUBTITLE
Low Temperature Deposition and Characterization of N- and P-Type Silicon Carbide Thin Films and Associated Ohmic and Schottky Contacts

6. AUTHOR(S)
Robert F. Davis and Robert J. Nemanich

5. FUNDING NUMBERS
sic0002---02
1261
N00179
N66005
4B855

7. PERFORMING ORGANIZATION NAME(S) AND ADDRESS(ES)
North Carolina State University
Hillsborough Street
Raleigh, NC 27695

8. PERFORMING ORGANIZATION REPORT NUMBER
N00014-92-J-1500

9. SPONSORING/MONITORING AGENCY NAMES(S) AND ADDRESS(ES)
Sponsoring: ONR, Code 1261, 800 N. Quincy, Arlington, VA 22217-5660
Monitoring: Administrative Contracting Officer, ONR Regional Office Atlanta
101 Marietta Tower, Suite 2805
101 Marietta Street
Atlanta, GA 30323-0008

10. SPONSORING/MONITORING AGENCY REPORT NUMBER

11. SUPPLEMENTARY NOTES

12a. DISTRIBUTION/AVAILABILITY STATEMENT

Approved for Public Release; Distribution Unlimited

12b. DISTRIBUTION CODE

13. ABSTRACT *(Maximum 200 words)*

Epitaxial, undoped films of 6H-SiC(0001) and 3C-SiC(111) have been grown by gas source (GS) MBE on 6H-SiC(0001) substrates and 2H-AlN(0001) layers between 1050-1250°C using SiH_4 and C_2H_4 for Si and C, respectively. Controlled n- and p-type doping was achieved via NH_3 and evaporated Al. REED and HRTEM showed the films to be monocrystalline and of either the 6H or 3C polytype. As-deposited (at RT) NiAl contacts with Ni passivating layers on p-type 6H-SiC(0001) substrates were rectifying with very low ρ_L (~1×10^{-8} A/cm² at 10 V), I_D values between 1.4 and 2.4, and a SBH of ≈1.37 eV. As-deposited (at RT) Ni and Au contacts on p-type 6H-SiC displayed similar C-V characteristics with SBH values of 1.31 and 1.27 eV, respectively. The Fermi level is partially pinned in p-type 6H-SiC. The Ni/NiAl contacts on p⁺ (1×10^{19} cm⁻³) 6H-SiC (0001) were ohmic after annealing for 10-80 s at 1000 °C in a N_2 ambient. The estimated specific contact resistivity from a non-mesa etched TLM pattern was $2-3\times10^{-2}$ W•cm⁻². Several boron compounds were selected as alternatives to Al materials. UPS measurements of $Al_{0.75}Ga_{0.25}N$ films deposited *in situ* via GSMBE and Si-doped GaN, $Al_{0.13}Ga_{0.87}N$ and $Al_{0.55}Ga_{0.45}N$ films deposited *ex situ* via OMVPE on 6H-SiC(0001) exhibited NEA characteristics in the former material, but not in the latter three samples. Annealing of the $Al_{0.55}Ga_{0.45}N$ sample to >400°C resulted in the disappearance of the sharp emission features. This effect was related to surface contamination. The results suggest the potential of nitride based cold cathode electron emitters. Al/AlN/α-SiC MIS diodes with several AlN thicknesses have been fabricated via GSMBE. C-V measurements at RT between 10 kHz and 1 MHz showed accumulation and depletion over the entire frequency range without dispersion. Inversion was not achieved. Thin layers (<1000Å) of AlN exhibited moderate leakage currents, but thicker layers reduced this problem. Calculated values of the dielectric constant matched the measured values.

14. SUBJECT TERMS
6H-SiC, 3C-SiC, AlN, gas source MBE, films, OMVPE, NiAl alloys, Ni, Al, rectifying, ohmic, Schottky barrier height, contact restivity, leakage current, Fermi level, UPS, AlGaN alloys, NEA, surface contamination, cold cathode, insulator, MIS diodes, C-V measurements, accumulation, depletion, dielectric constant

15. NUMBER OF PAGES
38

16. PRICE CODE

17. SECURITY CLASSIFICATION OF REPORT	18. SECURITY CLASSIFICATION OF THIS PAGE	19. SECURITY CLASSIFICATION OF ABSTRACT	20. LIMITATION OF ABSTRACT
UNCLAS	UNCLAS	UNCLAS	SAR

Table of Contents

Accesion For		
NTIS CRA&I	☒	
DTIC TAB	☐	
Unannounced	☐	
Justification		
By		
Distribution /		
Availability Codes		
Dist	Avail and / or Special	
A-1		

I. Introduction

Silicon carbide (SiC) is a wide bandgap material that exhibits polytypism, a one-dimensional polymorphism arising from the various possible stacking sequences of the silicon and carbon layers. The lone cubic polytype, β-SiC, crystallizes in the zincblende structure and is commonly referred to as 3C-SiC. In addition, there are also approximately 250 other rhombohesdral and hexagonal polytypes [1] that are all classed under the heading of α-SiC. The most common of the α-SiC polytypes is 6H-SiC, where the 6 refers to the number of Si/C bilayers along the closest packed direction in the unit cell and the H indicates that the crystal structure is hexagonal.

Beta (3C)-SiC is of considerable interest for electronic applications that utilize its attractive physical and electronic properties such as wide bandgap (2.2 eV at 300K) [2], high breakdown electric field (2.5×10^6 V/cm) [3], high thermal conductivity (3.9 W/cm °C) [4], high melting point (3103K at 30 atm) [5], high saturated drift velocity (2×10^7 m/s) [6], and small dielectric constant (9.7) [7]. Primarily due to its higher electron mobility than that of the hexagonal polytypes, such as 6H-SiC [8], β-SiC remains preferable to hexagonal SiC for most device applications.

Most 3C-SiC thin film growth to date has been performed on Si substrates. Large-area, crack-free, and relatively thick (up to 30 μm) epitaxial 3C-SiC thin films have been grown on Si (100) by exposing the Si substrate to a C-bearing gaseous species prior to further SiC growth [7, 9, 10]. However, these films exhibited large numbers of line and planar defects due to large lattice and thermal mismatches between SiC and Si. One particular type of planar defect, the inversion domain boundary (IDB), was eliminated with the use of Si (100) substrates cut 2°–4° toward [011] [11–13]. Growth on Si substrates has allowed much understanding of SiC growth processes and device development to occur, but the large thermal and lattice mismatches between SiC and Si hamper further development using Si substrates. As a result, great effort has been made to develop methods for growth SiC single crystal substrates for homoepitaxial growth of SiC thin films.

Since the 1950's, monocrystalline single crystals of 6H-SiC have been grown at using the Lely sublimation process [14]. However, nucleation was uncontrolled using this process and control of resultant polytypes was difficult. SiC single crystals inadvertently formed during the industrial Acheson process have also been used as substrates for SiC growth. However, neither these crystals or those formed using the Lely process are large enough for practical device applications. Recently, using a seeded sublimation-growth process, boules of single polytype 6H-SiC of > 1 inch diameter of much higher quality of that obtained using the Lely process have been grown. The use of single crystals of the 6H polytype cut from these boules has given a significant boost to SiC device development.

Silicon carbide epitaxial thin film growth on hexagonal SiC substrates has been reported since the 1960's. The use of nominally on-axis SiC substrates has usually resulted in growth of 3C-SiC films. Films of 3C-SiC (111) grown by CVD have been formed on 6H-SiC substrates less than 1° off (0001) [15]. Films of 3C-SiC on 6H-SiC substrates have typically had much lower defect densities than those grown on Si substrates. The major defects present in 3C-SiC/6H-SiC films have been double positioning boundaries (DPB) [16]. Despite the presence of DPBs, the resultant material was of sufficient quality to further device development of SiC. The use of off-axis 6H-SiC (0001) substrates has resulted in growth of high-quality monocrystalline 6H-SiC layers with very low defect densities [17].

In addition, the use of more advanced deposition techniques, such as molecular beam epitaxy (MBE), has been reported for SiC in order to reduce the growth temperature and from about 1400–1500°C on 6H-SiC substrates. Si and C electron-beam sources have been used to epitaxially deposit SiC on 6H-SiC (0001) at temperatures of 1150°C [18]. Ion-beam deposition of epitaxial 3C-SiC on 6H-SiC has also been obtained at the temperature of 750°C using mass-separated ion beams of $^{30}Si^+$ and $^{13}C^+$ [19].

Aluminum nitride (AlN) is also of particular interest at this time because of its very large bandgap. It is the only intermediate phase in the Al-N system and normally forms in the wurtzite (2H-AlN) structure. Most current uses of AlN center on its mechanical properties, such as high hardness (9 on Mohs scale), chemical stability, and decomposition temperature of about 2000°C [20]. Properties such as high electrical resistivity (typically $\geq 10^{13}$ Ω-cm), high thermal conductivity (3.2 W/cm K) [21], and low dielectric constant ($\varepsilon \approx 9.0$) make it useful as a potential substrate material for semiconductor devices as well as for heat sinks. The wurtzite form has a bandgap of 6.28 eV [22] and is a direct transition, thus it is of great interest for optoelectronic applications in the ultraviolet region.

Because of the difference in bandgaps (2.28 eV for 3C-SiC; 3.33 eV for 2H-SiC and 6.28 eV for 2H-AlN) between the materials, a considerable range of wide bandgap materials, made with these materials, should be possible. Two procedures for bandgap engineering are solid solutions and multilayers. A particularly important factor is that the two materials have a lattice mismatch of less than one percent.

Research in ceramic systems suggests that complete equilibrium solid solubility of AlN in SiC may exist, but only above ≈2000°C [23]. However, these solutions should be possible using the very non equilibrium technique of MBE. Solid solutions of the wurtzite crystal structure should have E_g from 3.33 eV to 6.28 eV at 0 K. Although it has not been measured, the bandgap of cubic AlN has been estimated to be around 5.11 eV at absolute zero and is believed to be indirect [24]. Cubic solid solutions should thus have E_g from 2.28 eV to roughly 5.11 eV at 0 K and would be indirect at all compositions if theory holds true.

Because of their similarity in structure and close lattice and thermal match, AlN-SiC heterostructures are feasible for electronic and optoelectronic devices in the blue and infrared region. Monocrystalline AlN layers have been formed by CVD on SiC substrates [25] and SiC layers have been formed on AlN substrates formed by AlN sputtering on single crystal W [26]. In addition, theory on electronic structure and bonding at SiC/AlN interfaces [24] exists and critical layer thicknesses for misfit dislocation formation have been calculated for cubic AlN/SiC [27]. Note that AlN (at least in the wurtzite structure) is a direct-gap material and SiC is an indirect gap material. Superlattices of these materials would have a different band structure than either constituent element. The Brillouin zone of a superlattice in the direction normal to the interfaces is reduced in size. This reduction in zone size relative to bulk semiconductors causes the superlattice bands to be "folded into" this new, smaller zone. This folding can cause certain superlattice states to occur at different points in k space than the corresponding bulk material states [28]. This can lead to direct transitions between materials which in the bulk form have indirect transitions. This has been demonstrated in the case of $GaAs_{0.4}P_{0.6}$/GaP and $GaAs_{0.2}P_{0.8}$/GaP superlattices, where both constituents are indirect in the bulk form [29]. Whether this is possible in the case of AlN/SiC is unknown, but very intriguing. It may be possible to obtain direct transitions throughout nearly the entire bandgap range with use of superlattices of AlN and SiC. Use of solid solutions in superlattices introduces additional degrees of freedom. For example, the bandgap can be varied independently of the lattice constant with proper choice of layer thickness and composition if superlattices of solid solutions of AlN and SiC were formed.

Due to the potential applications of solid solutions and superlattice structures of these two materials, an MBE/ALE system was commissioned, designed, and constructed for growth of the individual compounds of SiC and AlN, as well as solid solutions and heterostructures of these two materials. Chemical interdiffusion studies concerned with the kinetics and mechanisms of mass transport of Si, C, Al and N at the SiC/AlN interface are also being conducted in tandem with the deposition investigations.

A very important additional goal of this research is to understand what controls the contact electrical characteristics of specific metals to n-type and p-type 6H-SiC(0001) and to use this information to form good ohmic and Schottky contacts. Several metals and alloys have been and will be studied. The selection process began by taking the simplest case, an ideal contact which behaves according to Schottky-Mott theory. This theory proposes that when an intimate metal-semiconductor contact is made the Fermi levels align, creating an energy barrier equal to the difference between the work function of the metal and the electron affinity of the semiconductor. It is the height of this barrier which determines how the contact will behave; for ohmic contacts it is desirable to have either no barrier or a negative barrier to electron flow, while for a good Schottky contact a large barrier is desired.

3

Although the contact materials have been chosen optimistically, i.e. on the basis that they will form ideal contacts, some evidence exists that the contact properties will be more complicated. J. Pelletier *et al.* [30] have reported Fermi level pinning in 6H-SiC due to intrinsic surface states, suggesting little dependence of barrier height on the work function of the metal. In addition, L. J. Brillson [31, 32] predicts the pinning rate to be higher for more covalently bonded materials. Other complications may arise if the surface is not chemically pristine. A major part of this project is devoted to determining whether the contacts behave at all ideally, and if not, whether the Fermi level is pinned by intrinsic or extrinsic effects.

Along with examining the barriers of the pure metal contacts, the chemistry upon annealing is also being studied and correlated with the resulting electrical behavior. The electrical behavior is also quantified both macroscopically in terms of current-voltage characteristics and microscopically in terms of barrier height. The identification of the phases formed at the interface during deposition or subsequent annealing are determined using high resolution analytical TEM. Changes in the interface microstructure are also being correlated with the electrical characteristics of the contacts.

Within this reporting period, investigations concerned with (1) growth and doping of monocrystalline epitaxial films of β(3C)-SiC(111) and α(6H)-SiC(0001) on α(6H)-SiC(0001) and 2H AlN substrates via gas-source GSMBE, (2) UV photoemission from GaN and AlGaN alloys, (3) the deposition and characterization of new ohmic and rectifying contacts to p-type 6H-SiC and (4) fabrication by GSMBE and electrical characterization of Al/AlN/SiC MIS diodes.

The experimental procedures, results, discussion of these results, conclusions and plans for future efforts for each of the topics noted above are presented in the following sections. Each of these sections is self-contained with its own figures, tables and references.

References

1. G. R. Fisher and P. Barnes, Philos. Mag. B **61**, 217 (1990).
2. H. P. Philipp and E. A. Taft, in *Silicon Carbide, A High Temperature Semiconductor*, edited by J. R. O'Connor and J. Smiltens (Pergamon, New York, 1960), p. 371.
3. W. von Muench and I. Pfaffender, J. Appl. Phys. **48**, 4831 (1977).
4. E. A. Bergemeister, W. von Muench, and E. Pettenpaul, J. Appl. Phys. **50**, 5790 (1974).
5. R. I. Skace and G. A. Slack, in *Silicon Carbide, A High Temperature Semiconductor*, edited by J. R. O'Connor and J. Smiltens (Pergamon, New York, 1960), p. 24.
6. W. von Muench and E. Pettenpaul, J. Appl. Phys. **48**, 4823 (1977).
7. S. Nishino, Y. Hazuki, H. Matsunami, and T. Tanaka, J. Electrochem Soc. **127**, 2674 (1980).
8. P. Das and K. Ferry, Solid State Electronics **19**, 851 (1976).
9. K. Sasaki, E. Sakuma, S. Misawa, S. Yoshida, and S. Gonda, Appl. Phys. Lett. **45**, 72 (1984).
10. P. Liaw and R. F. Davis, J. Electrochem. Soc. **132**, 642 (1985).
11. K. Shibahara, S. Nishino, and H. Matsunami, J. Cryst. Growth **78**, 538 (1986).

12. J. A. Powell, L. G. Matus, M. A. Kuczmarski, C. M. Chorey, T. T. Cheng, and P. Pirouz, Appl. Phys. Lett. **51**, 823 (1987).
13. H. S. Kong, Y. C. Wang, J. T. Glass, and R. F. Davis, J. Mater. Res **3**, 521 (1988).
14. J. A. Lely, Ber. Deut. Keram. Ges. **32**, 229 (1955).
15. H. S. Kong, J. T. Glass, and R. F. Davis, Appl. Phys. Lett. **49**, 1074 (1986).
16. H. S. Kong, B. L. Jiang, J. T. Glass, G. A. Rozgonyi, and K. L. More, J. Appl. Phys. **63**, 2645 (1988).
17. H. S. Kong, J. T. Glass, and R. F. Davis, J. Appl. Phys. **64**, 2672 (1988).
18. S. Kaneda, Y. Sakamoto, T. Mihara, and T. Tanaka, J. Cryst. Growth **81**, 536 (1987).
19. S. P. Withrow, K. L. More, R. A. Zuhr, and T. E. Haynes, Vacuum **39**, 1065 (1990).
20. C. F. Cline and J. S. Kahn, J. Electrochem. Soc. **110**, 773 (1963).
21. G. A. Slack, J. Phys. Chem. Solids **34**, 321 (1973).
22. W. M. Yim, E. J. Stofko, P. J. Zanzucci, J. I. Pankove, M. Ettenberg, and S. L. Gilbert, J. Appl. Phys. **44**, 292 (1973).
23. See, for example, R. Ruh and A. Zangvil, J. Am. Ceram. Soc. **65**, 260 (1982).
24. W. R. L. Lambrecht and B. Segall, Phys. Rev. B **43**, 7070 (1991).
25. T. L. Chu, D. W. Ing, and A. J. Norieka, Solid-State Electron. **10**, 1023 (1967).
26. R. F. Rutz and J. J. Cuomo, in *Silicon Carbide-1973*, ed. by R. C. Marshall, J. W. Faust, Jr., and C. E. Ryan, Univ. of South Carolina Press, Columbia, p. 72 (1974).
27. M. E. Sherwin and T. J. Drummond, J. Appl. Phys. **69**, 8423 (1991).
28. G. C. Osbourn, J. Vac. Sci. Technol. B **1**, 379 (1983).
29. P. L. Gourley, R. M. Biefeld, G. C. Osbourn, and I. J. Fritz, *Proceedings of 1982 Int'l. Symposium on GaAs and Related Compounds* (Inst. Physics, Berkshire, 1983), p. 248.
30. J. Pelletier, D. Gervais, and C. Pomot, J. Appl. **55**, 994 (1984).
31. L. J. Brillson, Phys. Rev. B **18**, 2431 (1978).
32. L. J. Brillson, Surf. Sci. Rep. **2**, 123 (1982).

II. Electrical Characterization of SiC Grown by Gas-source Molecular Beam Epitaxy

A. Introduction

Silicon carbide (SiC) is a wide bandgap material that exhibits polytypism, a one-dimensional polymorphism arising from the various possible stacking sequences of, e. g., the silicon and carbon layers along the directions of closest packing. There are approximately 250 SiC polytypes [1]. Included in these is one cubic polytype. This single cubic polytype, β-SiC, crystallizes in the zincblende structure, has a room temperature bandgap of 2.3 eV, and is commonly referred to as 3C-SiC. (In the Ramsdell notation, the three (3) refers to the number of Si and C bilayers necessary to produce a unit cell and the C indicates its cubic symmetry.) The other rhombohedral and hexagonal polytypes are classed under the heading of α-SiC. The most common of these latter polytypes is 6H-SiC with a room temperature bandgap of ≈ 3.0 eV.

Since the 1950's, monocrystalline single crystals of 6H-SiC have been grown using the Lely sublimation process [2]. However, nucleation was uncontrolled using this process and control of resultant polytypes was difficult. In the last decade, using a seeded sublimation-growth process, commercial wafers cut from boules of single polytype 6H-SiC of >1 inch diameter have been grown of much higher quality than that obtained using the Lely process. The use of single crystals of the 6H polytype cut from these boules has given a significant boost to SiC research and device development.

Silicon carbide epitaxial thin film growth on hexagonal SiC substrates has been reported since the 1960's. The use of nominally on-axis SiC substrates has usually resulted in growth of 3C-SiC films. Films of 3C-SiC(111) grown by CVD have been formed on 6H-SiC substrates less than 1° off (0001) [3]. Films of 3C-SiC on 6H-SiC substrates have typically had much lower defect densities than those grown on Si substrates. The major defects present in β-SiC/6H-SiC films have been double positioning boundaries (DPB) [4]. Despite the presence of DPBs, the resultant material was of sufficient quality to further device development of SiC. The use of off-axis 6H-SiC(0001) substrates has resulted in growth of high-quality monocrystalline 6H-SiC layers with very low defect densities [5].

In addition, the use of more advanced deposition techniques, such as molecular beam epitaxy (MBE), has been reported for SiC in order to reduce the growth temperature from about 1400-1800°C on 6H-SiC substrates. Silicon and C electron-beam sources have been used to epitaxially deposit SiC on 6H-SiC (0001) at temperatures of 1150°C [6].

B. Experimental Procedure

Thin, epitaxial films of SiC were grown on the Si face of 6H-SiC(0001) substrates supplied by Cree Research, Inc. These included both vicinal 6H-SiC(0001) wafers oriented

6

3-4° towards [11$\bar{2}$0] containing a 0.75 μm epitaxial 6H-SiC layer deposited via CVD and on-axis 6H-SiC(0001) wafers. All wafers were received with a thermally oxidized 75 nm layer to aid in wafer cleaning. Wafers are prepared for growth by a 10% HF dip and a 10 minute anneal at 1050°C in UHV as well as a silane exposure and boil-off, a technique detailed in previous reports and based on the work of Kaplan [7].

All films were grown using a specially designed and previously described [8] GSMBE system. The base and operating pressures were 10^{-9} Torr and 10^{-3}–10^{-6} Torr, respectively. All films were grown between 1050–1500°C using different ratios of silane (SiH_4, 99.999% purity) and ethylene (C_2H_4, 99.99% purity) with total source inputs ranging from 0.6-2.0 sccm on both vicinal and on-axis α(6H)-SiC(0001). Similar to the results described in the previous report, 6H-SiC films were produced only when >5.0 sccm H_2 were included in the reactant gas flow and the substrate temperature was maintained at >1350°C. Thin 2H-AlN(0001) buffer layers, grown on on-axis α(6H)-SiC(0001), were also used as substrates for 3C-SiC(111) layers. The thin AlN layers were grown for 1 minute in the same system at 1050°C using a standard Al (99.9999% purity) effusion cell source, operating at 1250°C, and a compact electron cyclotron resonance (ECR) source to activate 3.5 sccm of N_2 (99.9995% purity). (This procedure has been described previously [10, 11]). For the purposes of the doping studies, the 6H polytype, grown on vicinal 6H-SiC, was investigated. Solid aluminum, evaporated from a standard MBE effusion cell, was used for p-type doping and ammonia (NH_3, diluted to 300 ppm in H_2) was used for n-type doping.

Reflection high-energy electron diffraction (RHEED) at 10 kV and high-resolution transmission electron microscopy (HRTEM) were used for structural and microstructural analyses. Samples were prepared for HRTEM using standard techniques [11]. A Topcon EM 002B high-resolution transmission electron microscope was used at 200 kV for the HRTEM analysis. Secondary ion mass spectrometry (SIMS), using both a Cameca IMS-3f and a UHV-compatible Cameca IMS-4f ion microprobe operating at 10 keV, was employed to determine the atomic concentrations of H, O, N and Al. Carrier concentrations for undoped SiC films, grown on insulating AlN layers, as well as p-type and n-type doped films were measured at room temperature by C-V and by standard Hall techniques at 3.5 kG. Nickel contacts, RF sputtered at room temperature then annealed at 1000°C for 30 s in Ar, were used on the undoped and n-type films and aluminum contacts, evaporated in a standard evaporator and annealed at 500°C for 30 seconds in Ar, were used on p-type films.

C. Results

Undoped films of α(6H)-SiC(0001) have been grown on vicinal 6H-SiC(0001) substrates at temperatures above 1350 °C. Optimum conditions for growth were determined to be a substrate temperature of 1450 °C using 0.6 sccm SiH_4 and either 0.375 or 0.6 sccm C_2H_4.

Growth rates approaching 1500 Å per hour were achieved. C-V and Hall electrical measurements made on some of the thicker SiC films (≈ 1.0 μm) have shown the films to be n-type with electron concentrations as low as 6×10^{14} cm^{-3} and mobilities as high as 72 cm^{2}V^{-1}s^{-1}. Figure 1 shows a typical SIMS profile of a MBE epilayer on top of a CVD epilayer. While both layers are of comparable structural quality, the MBE layer has a considerably lower concentration of residual nitrogen.
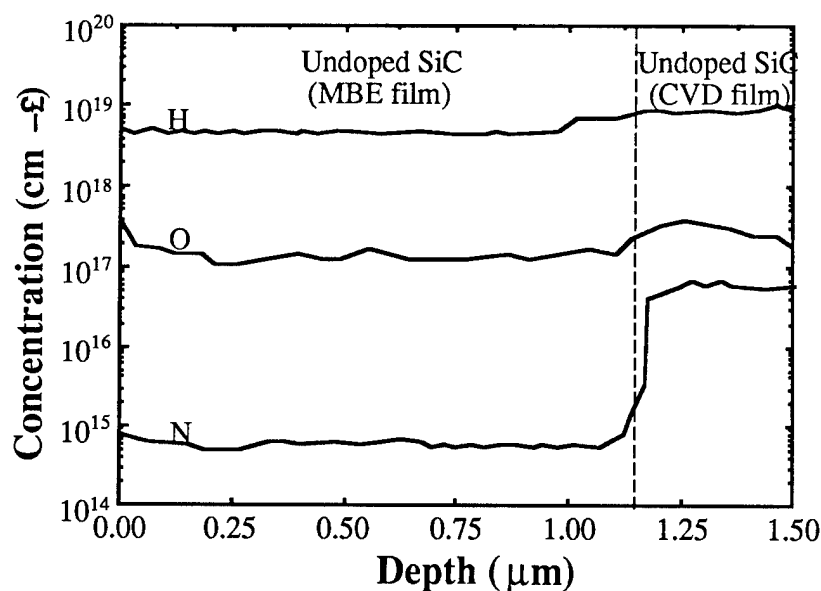

Figure 1.   SIMS profile of a MBE epilayer grown on a CVD epilayer. Note the reduced nitrogen content in the MBE layer.

Undoped films of β-SiC(111) have been grown on thin, insulating layers of 2H-AlN(0001) at 1350°C using 0.6 sccm SiH$_4$ and 0.6 sccm C$_2$H$_4$. Growth was initiated at 1100 °C and the temperature was increased to 1350 °C at a rate of 10 °C min^{-1}. Growth rates approaching those achieved for homoepitaxial growth of SiC on vicinal SiC were measured. C-V and Hall electrical measurements made on some of the thicker SiC films (≈ 1.0 μm) have shown the films to be n-type with electron concentrations as low as 2×10^{15} cm^{-3} and mobilities as high as 681 cm^{2}V^{-1}s^{-1}. Figure 2 shows a typical SIMS profile of a MBE epilayer on top of an AlN layer grown on a CVD epilayer. While both SiC layers are of comparable quality (though different polytypes), the MBE layer has a considerably lower concentration of residual nitrogen.

P-type Doping. Homoepitaxial SiC films on n-type substrates were doped p-type with Al at several different impurity concentrations. Carrier concentrations were measured on a number of Al-doped 6H-SiC films by C-V and the Hall technique. These films were grown under the previously stated conditions. Four different doping levels were achieved with Al effusion cell
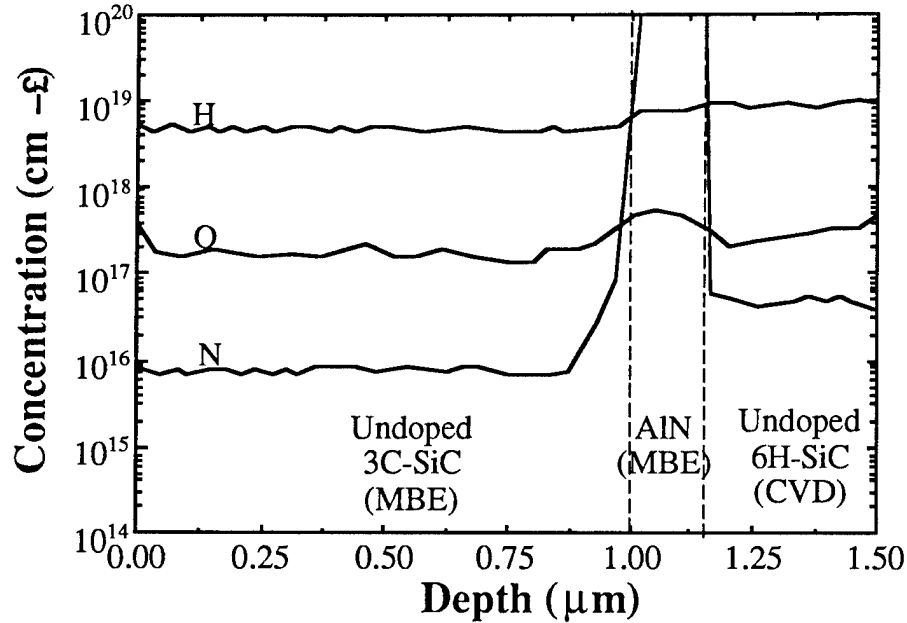
Figure 2. SIMS profile of a MBE epilayer grown on an AlN layer on a CVD epilayer. Note the reduced nitrogen content in the MBE layer.

temperatures held at 770°C, 840°C, 920°C and 1010°C. The Hall results are shown in Table I. Figure 3 shows SIMS profiles for the same p-type films as displayed in Table I. Compared to our previously reported [12] p-type doped films, these profiles are very smooth and uniform.

Table I. Hall Concentrations and Mobilities of Various P-type SiC Films

Aluminum Cell Temperature (°C)	Hole Concentration (cm^{-3})	Hole Mobility (cm^{2}V^{-1}s^{-1})
770	4.6×10^{15}*	N/A
840	6.7×10^{16}	30
920	8.7×10^{17}	24
1010	9.1×10^{18}	18

* Too resistive for Hall characterization. Carrier concentration determined by C-V.

N-type Doping. Homoepitaxial SiC films on p-type substrates were doped n-type using NH$_3$, diluted to 300 ppm in H$_2$, at several different impurity concentrations. Carrier concentrations were measured on a number of N-doped 6H-SiC films by C-V and the Hall
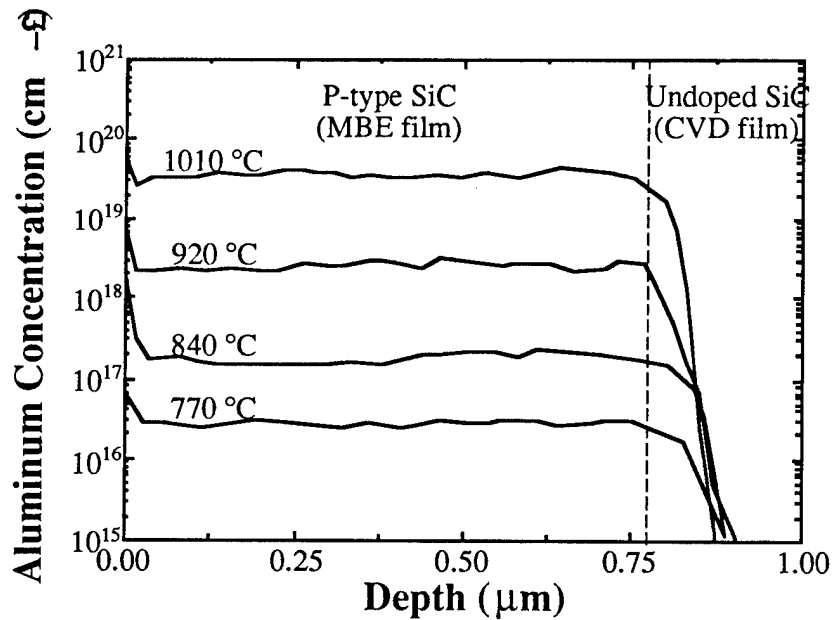
Figure 3.   SIMS profiles for 6H-SiC films doped with Al from an MBE effusion cell at different source temperatures.

technique. These films were grown under the previously-stated conditions. Three different doping levels were achieved with NH_3/H_2 flow rates at 0.08, 0.6 and 5.0 sccm. The Hall results are shown in Table II. Figure 4 shows SIMS profiles for the same n-type films as displayed in Table II.

Table II. Hall Concentrations and Mobilities of Various N-type SiC Films

NH_3/Ar Flow Rate (sccm)	Electron Concentration (cm^{-3})	Electron Mobility $(cm^2V^{-1}s^{-1})$
0.08	1.8×10^{15}	58
0.60	2.1×10^{16}	41
5.00	9.8×10^{17}	26

D.   Discussion

The results of the Hall measurements on undoped β-SiC, grown on AlN on on-axis 6H-SiC, represent some of the lowest unintentional doping levels ever reported in the cubic polytype. Molecular beam epitaxy is also shown to produce very pure layers with very low
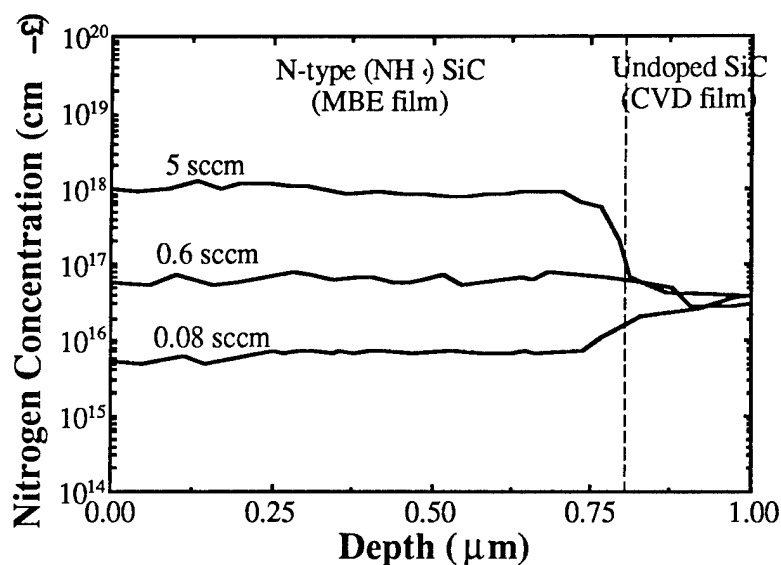
Figure 4. SIMS profiles for 6H-SiC films doped with N from an NH_3/H_2 mix.

impurity concentrations. The Hall measurements listed in Tables I and II and the SIMS data displayed in Figs. 3 and 4 represent the first intensive attempt at SiC doping ever attempted by MBE. As expected, the concentration of both impurity atoms and carriers increased as the source flux increased. The profiles in Fig. 3 and the data in Table I are of the same order of magnitude indicating a much higher activation efficiency in p-type SiC than previously reported by CVD [13]. Similar data are also shown for the n-type samples.

E. Conclusions

Films of 6H- and 3C-SiC have been grown between 1050-1500°C by GSMBE using SiH_4 and C_2H_4 on different orientations of α(6H)-SiC(0001) and on thin buffer layers of AlN. Growth of SiC on AlN represents a possible means of growing higher quality β-SiC(111) than previously reported. Hall electrical measurements on these films revealed carrier concentrations as low as 2×10^{15} cm^{-3} and room temperature mobilities as high as 681 cm^{2}V^{-1}s^{-1}.

Doped films of 6H-SiC have been grown on vicinal α(6H)-SiC(0001) at T>1350°C. The films (doped p-type with Al and n-type with N) showed carrier concentrations that increased with increasing impurity flux. SIMS profiles for Al incorporation are of the same order of magnitude indicating a much higher activation efficiency than previously reported by CVD.

F. Future Research Plans and Goals

Further work on doping both 3C- and 6H-SiC will be performed. Studies related to the doping of SiC with N_2 will be initiated. Additionally, further studies will be initiated to study

the role that hydrogen and other gases may play in the activation efficiency of carriers in SiC films. Hydrogen incorporation is postulated [14] as a possible retardant to impurity activation.

G. References

1. G. R. Fisher and P. Barnes, Philos. Mag. B **61**, 217 (1990).
2. J. A. Lely, Ber. Deut. Keram. Ges. **32**, 229 (1955).
3. H. S. Kong, J. T. Glass, and R. F. Davis, Appl. Phys. Lett. **49**, 1074 (1986).
4. H. S. Kong, B. L. Jiang, J. T. Glass, G. A. Rozgonyi, and K. L. More, J. Appl. Phys. **63**, 2645 (1988).
5. H. S. Kong, J. T. Glass, and R. F. Davis, J. Appl. Phys. **64**, 2672 (1988).
6. S. Kaneda, Y. Sakamoto, T. Mihara, and T. Tanaka, J. Cryst. Growth **81**, 536 (1987).
7. R. Kaplan, Surface Sci. **215**, 111 (1989).
8. L. B. Rowland, S. Tanaka, R. S. Kern and R. F. Davis, in *Proceedings of the Fourth International Conference on Amorphous and Crystalline Silicon Carbide and Related Materials*, edited by C. Y. Yang, M. M. Rahman and G. L. Harris (Springer-Verlag, Berlin, 1992) p. 84.
9. L. B. Rowland, R. S. Kern, S. Tanaka and R. F. Davis, J. Mater. Res. **8**, 2310 (1993).
10. L. B.Rowland, R. S. Kern, S. Tanaka and R. F. Davis, Appl. Phys. Lett. **62**, 3333 (1993).
11. S. P. Withrow, K. L. More, R. A. Zuhr, and T. E. Haynes, Vacuum **39**, 1065 (1990).
12. R. S. Kern, S. Tanaka and R. F. Davis, in *Transactions of the Second International High Temperature Electronics Conference* (1994) p. P-141.
13. H. J. Kim and R. F. Davis, J. Electrochem. Soc. **133**, 2350 (1986).
14. E. Bringuier, personal communication.

III. Rectifying and Ohmic Contacts for P-type Alpha (6H) Silicon Carbide

A. Introduction

While the wide bandgap of SiC is responsible for its use in opto-electronic, high-power, and high-temperature devices, this property also adds to the difficulty of controlling the electrical properties at the metal-semiconductor contacts in these devices. The primary parameter used to quantify the electrical relationship at these interfaces is the Schottky barrier height (SBH), or the energy barrier for electrons traversing the interface. A small SBH is desired for a contact which obeys Ohm's Law, while a relatively large SBH is necessary to create a good rectifying contact.

The formation of low resistivity and thermally stable ohmic contacts to 6H-SiC remains a serious problem in the development of SiC device technology. For SiC power devices to have the advantage over Si, the contact resistivities must be below 1×10^{-5} Ω-cm^2 [1]. In addition, the electrical characterization of state-of-the-art SiC films depends on the ability to fabricate ohmic contacts on material with low carrier concentrations. Therefore, better ohmic contacts are needed both for improving device performance and for improving the quality of films which can be grown. The thermal stability of ohmic contacts is of particular concern for p-type SiC, which have traditionally relied on Al or Al alloys to dope the SiC surface below the contacts. While the fabrication of ohmic contacts to SiC also has usually depended on very heavily-doped surfaces, the introduction of high levels of dopants in the near surface device region of the epilayer prior to the deposition of the contact or by ion implantation through the contact makes probable the introduction of point and line defects as a result of the induced strain in the lattice. Based on all of these issues and experiments already performed at NCSU, our goals are to produce contacts which are thermally stable and have low contact resistivities while also reducing the need for doping by ion implantation.

Low resistance contacts to p-type SiC remain a substantial challenge for high temperature and high-power devices. An Al-Ti alloy [2] annealed at 1000°C for 5 min. was reported to yield contact resistances ranging from 2.9×10^{-2} Ω cm^2 for a carrier concentration of 5×10^{15} cm^{-3} to 1.5×10^{-5} Ω cm^2 for 2×10^{19} cm^{-3}. The thermal stability of these contacts was not reported. Aluminum deposited on a heavily-doped 3C-SiC interlayer on a 6H-SiC substrate and subsequently annealed at 950°C for 2 min. reportedly yielded contact resistivities of $2-3 \times 10^{-5}$ Ω cm^2 [3]. Because of its low melting point (660°C), however, pure Al would be unsuitable for high temperature applications. Platinum contacts annealed from 450 to 750°C in 100°C increments were also used as ohmic contacts to p-type SiC [4]. These contacts, which rely on the combination of a highly-doped surface and the high work function of Pt, have not been known to yield contact resistivities as low as those for the contacts containing Al.

B. Experimental Procedure

Vicinal, single-crystal 6H-SiC (0001) wafers provided by Cree Research, Inc. were used as substrates in the present research. The wafers were doped with N or Al during growth to create n- or p-type material, respectively, with carrier concentrations of $1-5 \times 10^{18}$ cm^{-3}. Homoepitaxial layers (1–5 µm thick) grown by chemical vapor deposition (CVD) were Al-doped with carrier concentrations ranging from 1×10^{16} to 1×10^{19} cm^{-3}. The surfaces were oxidized to a thickness of 500–1000 Å in dry oxygen. The substrates were simultaneously cleaned and the oxide layer etched from the surface using a 10 min. dip in 10% hydrofluoric acid, transferred into the vacuum system, and thermally desorbed at 700 °C for 15 min. to remove any residual hydrocarbon contamination.

A UHV electron beam evaporation system was used to deposit the NiAl and Ni films. After depositing 1000 Å of NiAl, 500–1000 Å of Ni was deposited as a passivating layer. Pure Ni (99.99%) and pure Al (99.999%) pellets were arc melted to form alloyed pellets of 50:50 atomic concentration for evaporation of NiAl. The films were deposited onto unheated substrates at a rate of 10–20 Å/s. The pressure during the depositions was between 5×10^{-9} and 5×10^{-8} Torr.

Circular contacts of 500 µm diameter were fabricated for electrical characterization by depositing the metal films through a Mo mask in contact with the substrate. Silver paste served as the large area back contact. For contact resistance measurements, TLM patterns [6] were fabricated by photolithography. The Ni/NiAl films were etched in phosphoric acid : acetic acid : nitric acid (12 : 2 : 3) at 50 °C (etch rate ≈ 30 Å/s). The contact pads were 300×60 µm with spacings of 5, 10, 20, 30 and 50 µm. Mesas in the substrate were not fabricated. All subsequent annealing was conducted in a N$_2$ ambient in a rapid annealing furnace.

Electrical characteristics were obtained from current-voltage and capacitance-voltage measurements. Current-voltage (I-V) measurements were obtained with a Rucker & Kolls Model 260 probe station in tandem with an HP 4145A Semiconductor Parameter Analyzer. Capacitance-voltage (C-V) measurements were taken with a Keithley 590 CV Analyzer using a measurement frequency of 1 MHz.

Auger electron spectroscopy (AES) was performed with a JEOL JAMP-30 scanning Auger microprobe. The films were sputtered with Ar ions at a beam current and voltage of 0.3 µA and 3 kV, respectively, to obtain composition profiles through the thickness of the films.

C. Results

Modifications to Deposition System. To better control the deposition of compounds for SiC contacts by electron beam deposition, a second Leybold Inficon film thickness monitor was installed in the UHV chamber. Linear motion shifts on both thickness monitors allowed the monitors to be moved relative to the location of the deposition sources. Cylindrical material

14

directors placed around the crystals were used to try to isolate the flux reaching the crystal from one deposition source while eliminating the flux from the other source. As of this writing preliminary results have shown that some cross-deposition of material is inevitable, but it can probably be kept low enough to give satisfactory estimates of the amount of each material deposited while running both sources simultaneously. The necessity of having two thickness monitors will be elaborated in the Future Plans and Goals section of this report.

Chemical Characterization of As-deposited Films. An Auger depth profile of a film deposited from the NiAl source showed that the overall composition remained relatively stable. The relative compositions of Ni and Al were calculated by referencing to pure Ni and pure Al standards and accounting for their corresponding sensitivity factors. The average atomic composition was approximately 50:50.

Schottky Contacts. In the as-deposited condition the Ni/NiAl contacts were rectifying on p-type SiC with carrier concentrations of 1.6×10^{16} and 3.8×10^{18} cm^{-3} in the epilayer. The sample with the lower carrier concentration displayed leakage current densities of $\sim 1 \times 10^{-8}$ A/cm^2 at 10 V and ideality factors between 1.4 and 2.4, while the latter sample displayed approximately five orders of magnitude higher leakage current densities and similar ideality factors. The average Schottky barrier heights (SBH's) calculated for the samples with the lower and higher carrier concentrations were 1.37 and 1.26 eV, respectively. The lower SBH calculated for the former sample is likely due to enhanced thermionic field emission through the upper energy region of the barrier because of the narrower depletion region. Hence, the 1.37 eV value is believed to be more accurate.

Similar results were obtained for as-deposited Ni and Au contacts on p-type ($2.1\text{–}4.5 \times 10^{16}$ cm^{-3}) 6H-SiC (0001). These samples displayed similar leakage currents and ideality factors of 1.3–2.1 and <1.1, respectively. From these measurements SBH's of 1.31 eV for the Ni contacts and 1.27 eV for the Au contacts were calculated. In comparison, as-deposited Ni on n-type (4.1×10^{16} cm^{-3}) 6H-SiC (0001) yielded ideality factors below 1.1, similar leakage current densities to those stated above, and SBH's of 1.14 eV and 1.21 eV calculated from I-V and C-V measurements, respectively.

Our measurements on p-type SiC have shown consistent differences from measurements on n-type 6H-SiC. The SBH's tended to be higher on p-type than on n-type material. While leakage currents for Au, NiAl, and Ni contacts on p-type 6H-SiC were comparable to Ni contacts on n-type 6H-SiC, the ideality factors were higher on p-type SiC. These ideality factors and SBH's are higher than for Ni contacts (and other previously studied contacts) on n-type 6H-SiC (0001). The higher ideality factors indicates that thermionic emission was not the dominant current transport mechanism in the p-type SiC and may indicate the occurrence of recombination at deep levels.

On the other hand, the relationship between the SBH's of the metals on p-type SiC and their respective work functions was similar to that which we previously found for n-type SiC. The calculated SBH's on p-type SiC are plotted vs. the metal work functions in Fig. 1. The work function for NiAl was taken to be the average of the work functions for pure Ni and pure Al since a value was not found in the literature for NiAl. The slope of the line fit to the empirical data was -0.16 as compared to a slope of -1.0 for the theoretical data. These results indicate that surface states on p-type 6H-SiC (0001) cause a partial pinning of the Fermi level, in agreement with the results of our previous, extensive study on n-type SiC.
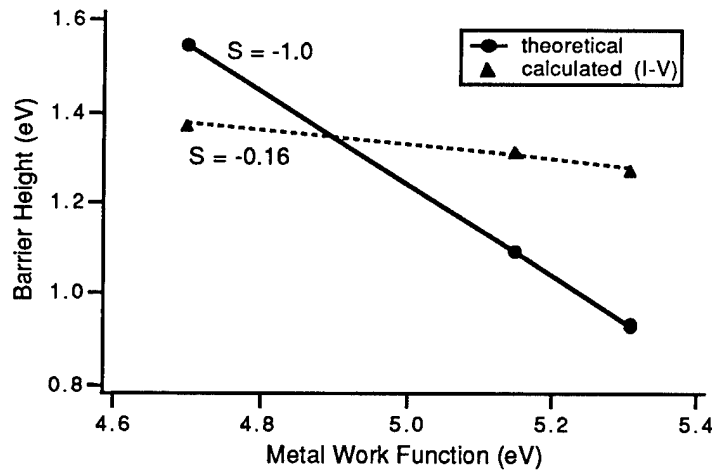

Figure 1.   Graph of calculated and theoretical barrier heights of as-deposited NiAl, Ni, and Au contacts on p-type 6H-SiC vs. metal work function. The calculated values were determined from I-V measurements, and the theoretical values were calculated according to the Schottky-Mott limit. The slopes, S, of the lines fit to each set of data are indicated on the graph.

Ohmic Contacts. The Ni/NiAl contacts were sequentially annealed for total times of 10–80 s at 1000 °C in a N_2 ambient. This temperature was used because (1) limited intermixing of Al and SiC was reported at 900 °C [7] and (2) other papers report annealing in this temperature range for Al-based ohmic contacts on p-type SiC [2, 3, 8]. Because of the extremely high thermodynamic driving force for Al to form an insulating oxide layer (ΔG_f (Al_2O_3) ~ -1300 kJ/mol at 1000 °C [JANAF - Chase, M., *et al.*, JANAF Thermochem. Tables, 3d Ed. J. Phys. Chem. Ref. Data, 1985. 14(Supp. 1)]), 1000 Å of Ni was deposited on top of the NiAl contacts to slow the oxidation process.

Table I summarizes the results of I-V measurements taken at selected intervals through the annealing series for three samples with various carrier concentrations in the SiC epitaxial layer (1.4×10^{18}, 5.7×10^{18}, and 1.5×10^{19} cm^{-3}). The two samples with the lower carrier concentrations were not truly ohmic but became ohmic-like after annealing for 80 s. This annealing series will be continued to determine whether ohmic behavior in these two samples

16

will ensue; however, the additional force on the probes needed to obtain consistent results indicates that an oxide has begun to form at the surface and may cause problems with further annealing. The sample with the higher carrier concentration was ohmic after annealing for 10 s. The calculated specific contact resistivity remained approximately 2.0×10^{-2} Ω cm^2 through annealing for 60 s. A slight increase to 3.1×10^{-2} Ω cm^2 was calculated after annealing for 80 s. This increase is believed to be due to the surface oxide layer.

Table I. Estimated specific contact resistivities / electrical behavior
of Ni (1000 Å) / NiAl (1000 Å) / p-SiC after annealing at 1000 °C for 20, 40, 60, and 80 s
for three samples with the carrier concentrations indicated. The specific contact resistivities
were calculated from non-mesa etched linear TLM patterns.

Annealing Time	20 s	40 s	60 s	80 s
1.4×10^{18} cm^{-3}	non-ohmic	non-ohmic	non-ohmic	almost ohmic
5.7×10^{18} cm^{-3}	non-ohmic	non-ohmic	non-ohmic	almost ohmic
1.5×10^{19} cm^{-3}	2.0×10^{-2} Ω cm^2	1.9×10^{-2} Ω cm^2	2.2×10^{-2} Ω cm^2	3.1×10^{-2} Ω cm^2

The high contact resistivities may be a result of a few causes. It is believed that the SiC may be depleted of carriers near the surface, possibly due to thermal oxidation. A depletion of carriers near the surface would result in higher than expected contact resistivity values because current transport across the contact depends on the carrier concentration in the SiC at the SiC surface. To investigate this potential problem we plan to compare the contacts described above with contacts on SiC implanted with Al and also on SiC which has not been thermally oxidized. The values of specific contact resistivity stated above should only be considered as preliminary estimates since only one level of the TLM measurement pattern was used. In the near future we plan to employ a circular TLM measurement structure [9], which consists of only one level and does not involve etching of the substrate. A photolithography mask for fabricating this structure was recently designed and fabricated at NCSU for this project.

D. Discussion

An Auger depth profile (Fig. 2b) of Ni/NiAl/SiC annealed at 1000 °C for 80 s shows that the surface oxide is thicker than that on the as-deposited sample (Fig. 2a). After sputtering for a couple of minutes, the O concentration dropped to below detectable limits; however, the data shows a decreasing Al concentration in the direction toward the SiC interface. This indicates that the kinetics are more favorable for the Al to diffuse toward the surface and react with O than for the Al to react with the SiC. Some of the Ni has probably reacted with Si at the interface to form a silicide, as indicated by the local maximum in the Ni intensity near the SiC interface, while the peak in the C intensity indicates the presence of an adjacent C-rich layer.
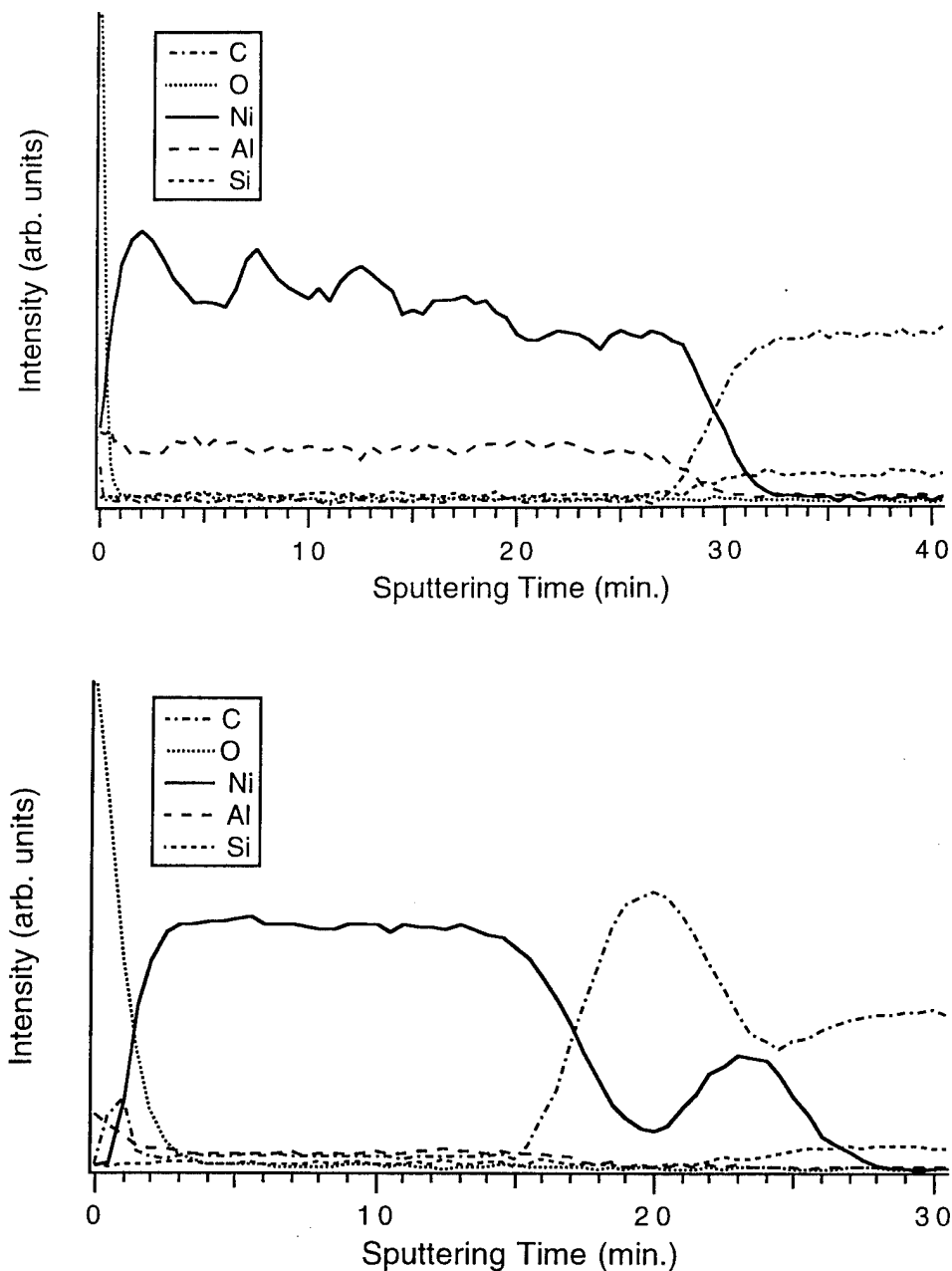
17

Figure 2.   AES composition profile of (a) NiAl (1000 Å) deposited at room temperature on (0001) 6H-SiC and (b) Ni (1000 Å) / NiAl (1000 Å) / 6H-SiC annealed at 1000 °C for 80 s in N_2.

The demonstrated oxidation problem with Al necessitates the development of ohmic contacts which do not consist of substantial concentrations of Al. To reduce this problem we have chosen to investigate selected materials which contain B as an alternative to Al.

The main reasons for choosing B are that it is also a p-type dopant in SiC, its oxide is not as stable, and it is a much faster diffusant in SiC. Table II compares some important properties of B, Al, and their associated oxides. Although the B acceptor level in 6H-SiC is substantially

18

deeper than that of Al, the fact that B is an acceptor makes it worth investigating as a component in p-type ohmic contacts. Also, boron compounds tend to be more stable at high temperatures than aluminum compounds which suffer from the low melting point of Al. As shown in Table II, the diffusion coefficient of B is at least three orders of magnitude greater than that of Al. Therefore, more B than Al will diffuse into the SiC at lower temperatures. As discussed in this report, a major problem with Al-based contacts is the strong driving force for forming an insulating oxide layer. This situation is shown by the extremely low equilibrium partial pressure, p_{O_2}, for Al_2O_3 formation. While B_2O_3 also has a low p_{O_2}, it is significantly higher than that for Al_2O_3, indicating that the driving force for B to form an oxide is significantly lower. In addition, the melting point of boron oxide is notably low.

Table II. Selected Properties of B, Al, and Their Associated Oxides

Element	Activation Energy in 6H-SiC (meV)	Solid Source Diffusion, D_{SiC} @ 1800°C (cm^2/s)	Equilibrium partial pressure of O_2, p_{O_2} @ 700°C (torr)	Melting temp. of the associated oxide, T_{melt} (°C)
B	700	10^{-11} [10-11]	10^{-35}	450
Al	240	$<10^{-14}$ [12]	10^{-47}	2040

Several boron compounds which possess reasonably low resistivities and high melting temperatures are listed in Table III. Of the compounds listed, the simplest to form by electron beam deposition would probably be CrB_2, VB_2, and ZrB_2. The refractory nature of these compounds increases the chance of forming ohmic contacts which will be stable at high temperatures.

Table III. Resistivities and Melting Points of Selected Boron Compounds

Compound	Electrical Resistivity ($\mu\Omega$-cm) 298 K [13]	Melting Temperature (°C) [14]
CrB_2	30	2200
GdB_4	31	2650
MoB	45	2600
NbB_2	26	3000
TaB_2	33	3037
VB_2	23	2747
ZrB_2	10	2972

E. Conclusions

Nickel-aluminum was investigated primarily as an ohmic contact for p-type 6H-SiC because of the p-type doping of Al in SiC, the high melting point of NiAl (as compared to Al), and the tendency of Ni to form silicides but not carbides. This latter property potentially could have resulted in extraction of Si from the SiC lattice in exchange for Al, thereby enhancing the p-type carrier concentration at the surface. Although the I-V measurements indicate that some Al may be diffusing into the SiC after the longest annealing time performed (80 s at 1000 °C), this potential for reaction between Al and SiC appears to be exceeded by the driving force for Al to diffuse to the surface and react with O. A concentration profile obtained from AES analysis shows that Al has diffused through the 1000 Å Ni overlayer to form a thin (200 Å estimated) oxide layer.

In addition to the ohmic behavior resulting from annealing the NiAl contacts, as-deposited Ni, NiAl, and Au contacts deposited at room temperature on p-type ($N_A < 5\times10^{16}$ cm^{-3}) 6H-SiC (0001) were rectifying with low leakage currents, ideality factors between 1.3 and 2.4, and SBH's of 1.31, 1.27, and 1.37 eV, respectively. These results indicate that the Fermi level is partially pinned at p-type SiC surface, in agreement with our previous results on n-type SiC.

An alternative to Al for fabricating ohmic contacts to 6H-SiC is the use of boron compounds. The metal borides listed in Table III are strong candidates for p-type SiC metallization because their low resistivities and high melting temperatures should allow the formation of high temperature contacts. Electron beam deposition of these materials ought to be possible.

F. Future Research Plans and Goals

The position of the two crystal thickness monitors during simultaneous electron beam deposition needs to be optimized. First, the ratio of the actual thickness being deposited to the thickness read by each monitor needs to be determined. This can be accomplished by measuring the actual thickness deposited from familiar metal sources. With the completion of these system modifications to allow co-deposition of compound metal films, we are prepared to deposit B-based contacts as an alternative to Al-based metallization.

An attempt to fabricate ohmic contacts to p-type SiC using boron compounds will be made. The deposition of some of the low resistivity, refractory borides listed previously in Table III will be carried out by electron beam evaporation. Careful electrical characterization needs to be performed to determine if annealing will improve the contact properties. In addition, the deposited films will be chemically analyzed by Auger electron spectroscopy to determine if the proper phases form.

Another alternate approach to Al-based ohmic contacts for p-type SiC will incorporate p-type semiconducting interlayers. The goal of this approach is to find a semiconducting

20

material which has a favorable band lineup with SiC (i.e., reduce the band bending) and to which an ohmic contact can easily be made. We have chosen to examine the $In_xGa_{1-x}N$ system for interlayer materials because of the lower density of surface states (and hence less band bending) and the range of bandgaps over the composition range. It is planned to measure the valence band offsets and electrical characteristics between various compositions of $In_xGa_{1-x}N$ (starting with x=0) and SiC. If a low energy barrier at the interface results, metals will be investigated for ohmic contacts for the interlayer / SiC structure.

To extend the study on NiAl ohmic contacts for p-type SiC, the contact resistivities for annealing series at 1000 °C will be repeated using circular TLM patterns and two different substrates: 1) SiC implanted with Al to increase the surface carrier concentration and 2) SiC which has not been thermally oxidized to investigate whether the bulk carrier concentration can be maintained at the surface. A photolithography mask with the circular TLM patterns was recently designed and will be used in the research on ohmic contacts in the very near future.

G. References

1. D. Alok, B. J. Baliga, and P. K. McLarty, IEDM Technical Digest **IEDM 1993**, 691 (1993).
2. J. Crofton, P. A. Barnes, J. R. Williams, and J. A. Edmond, Appl. Phys. Lett. **62**(4), 384 (1993).
3. V. A. Dmitriev, K. Irvine, and M. Spencer, Appl. Phys. Lett. **64**(3), 318 (1994).
4. R. C. Glass, J. W. Palmour, R. F. Davis, and L. S. Porter, U.S Patent No. 5,323,022 (1994).
5. J. L. Murray, Ed. *Phase Diagrams of Binary Titanium Alloys* (ASM International, Metals Park, Ohio, 1987).
6. H. H. Berger, Solid State Electronics **15**(2), 145 (1972).
7. V. M. Bermudez, J. Appl. Phys. **63**(10), 4951 (1988).
8. T. Nakata, K. Koga, Y. Matsushita, Y. Ueda, and T. Niina, in *Amorphous and Crystalline Silicon Carbide and Related Materials II*, M. M. Rahman, C. Y.-W. Yang, and G. L. Harris, Eds., Vol. 43 (Springer-Verlag, Berlin, 1989).
9. G. K. Reeves, Solid State Electronics **21**, 801 (1978).
10. E.N. Mokhov, Y.A. Vodakov, G.A. Lomakina, Soviet Physics - Solid State **11**(2), 415 (1969).
11. C. van Opdorp, Solid State Electronics **14**, 613 (1971).
12. E. Mokhov, Y. A. Vodakov, G. A. Lomakina, V. G. Oding, G. F. Kholuyanov, and V. V. Semenov, Soviet Physics - Semiconductors **6**(3), 414 (1972).
13 Samsonov, G. V. and I. M. Vinitskii, *Handbook of Refractory Borides*, (Plenum Press, New York, 1980).
14. *Binary Alloy Phase Diagrams, 2nd Ed.*, T. B. Massalski editor, (ASM International, 1990).

IV. UV Photoemission Study of Heteroepitaxial AlGaN Films Grown on 6H-SiC

A. Introduction

There is increasing interest in electronic devices composed of III-nitride materials for opto-electronic applications in the blue and UV region [1]. In order to construct viable optical devices, a knowledge of band offsets and electron affinity is needed. An alternative application of these semiconductors is in electron emission devices. Recent studies have demonstrated that diamond surfaces can exhibit a negative electron affinity (NEA). Negative electron affinity surfaces may prove to be critical elements for cold cathode devices, vacuum microelectronics, and photodetectors [2,3]. In addition to diamond, thin films of AlN grown on 6H SiC have been shown to exhibit a NEA and band offsets have been determined [4,5]. The AlN NEA surfaces were obtained from air-exposed surfaces and do not appear to be readily poisoned. In contrast to diamond, AlGaN materials exhibit the wurtzite crystal structure. One of the most significant limitations in the application of diamond is that reliable n-type doping has not been achieved. In contrast, n-type doping has been obtained for GaN and some AlGaN alloys. This study explores further the electron affinity of epitaxial AlGaN films on 6H-SiC.

The wurtzite AlN and GaN form a continuous solid solution of $Al_xGa_{1-x}N$ for $0 \leq x \leq 1$ with bandgaps that range from 3.4 eV (GaN) to 6.2 eV (AlN). Figure 1 displays the bandgap of several materials as a function of the equivalent hexagonal lattice constant. The alloys are also miscible with In, hence the inclusion of InN could extend the range to 1.9 eV. The InGaN alloys will be important in visible light applications. The electron affinity of a semiconductor is related to the surface dipole and to the fundamental energy levels of the materials. Because the valence and conduction bands of the semiconductors have origin in the sp^3 bonding and antibonding levels, it may be suggested that the larger bandgap materials will exhibit a smaller or negative electron affinity. In comparison with diamond, it might be assumed that AlGaN alloys with a bandgap greater than 5.4 eV could exhibit a NEA. Reported here are studies of AlGaN with x values of 0.55 and 0.13 as well as preliminary studies of GaN.

The AlGaN and GaN films used in this study were are grown on vicinal 6H-SiC substrates. The n-type SiC substrates used have a small lattice mismatch with AlN (3.08 Å vs. 3.11 Å) and GaN (a= 3.19Å). The small lattice mismatch enables heteroepitaxial growth of the wurtzite (2H) structure. Furthermore, the fact that the substrates are conducting avoids charging problems associated with photoemission from large bandgap and insulating materials.

The electron affinity of a semiconductor or the presence of a NEA can be determined by ultraviolet photoemission spectroscopy (UPS) [6-8]. The experiments described here involve directing 21.2 eV light (the He I resonance line) to the surface of the sample and detecting the
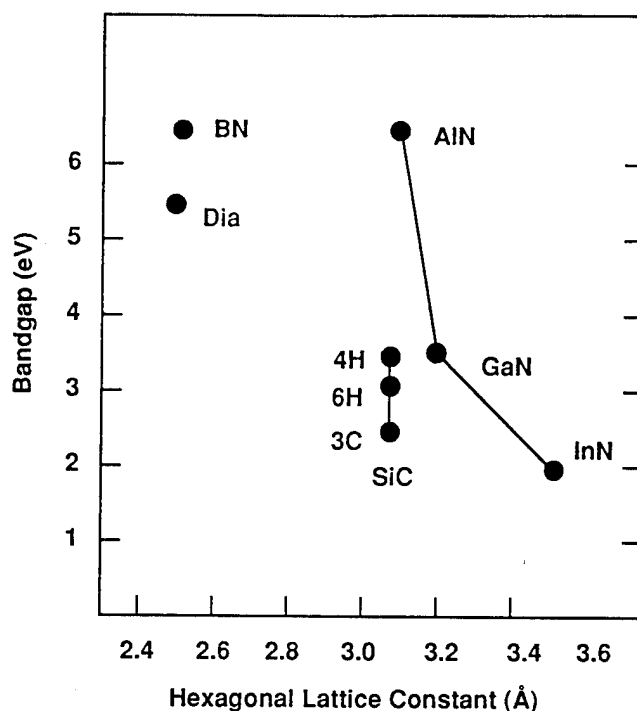
22

Figure 1.   The bandgap vs. hexagonal lattice constant (a) for a variety of wide bandgap
semiconductors. The lattice constant for the cubic materials has been determined
from the (111) plane.

spectrum of the emitted photo-excited electrons as a function of electron kinetic energy. Typically, UPS is used to obtain a profile of the valence band (VB) electronic states. As such, most studies of UPS of semiconductors present data of the most energetic electrons emitted from the surface. Electrons scattered to lower energy and secondary electrons will be displayed in the spectrum at lower kinetic energies. In addition, for a semiconductor which exhibits a NEA surface, a distinctive peak may be observed at the low kinetic energy (highest binding energy) end of the photoemission spectra. Figure 2 depicts a schematic representation of the photoemission spectra from a semiconductor with a negative or positive electron affinity. The low kinetic energy feature is due to secondary electrons which (quasi) thermalize to the conduction band minimum. Note that the solid line indicates a material with a positive electron affinity while the dashed line is a feature indicative of a NEA. In this paper, samples with both positive and negative affinity surfaces will be discussed.

The sharp features typical of a NEA have been observed from spectra of (111) and (100) diamond surfaces [6-10]. In the studies of diamond, a correlation was made between the presence of hydrogen and the NEA peak [9,10]. In addition, it was also shown that thin metal layers such as Ti or other moderate work function metals could induce a NEA on the diamond surface [10,11]. These measurements verify that the surface dipole can be influenced by surface processing and that the effects contribute to the observation of a NEA.
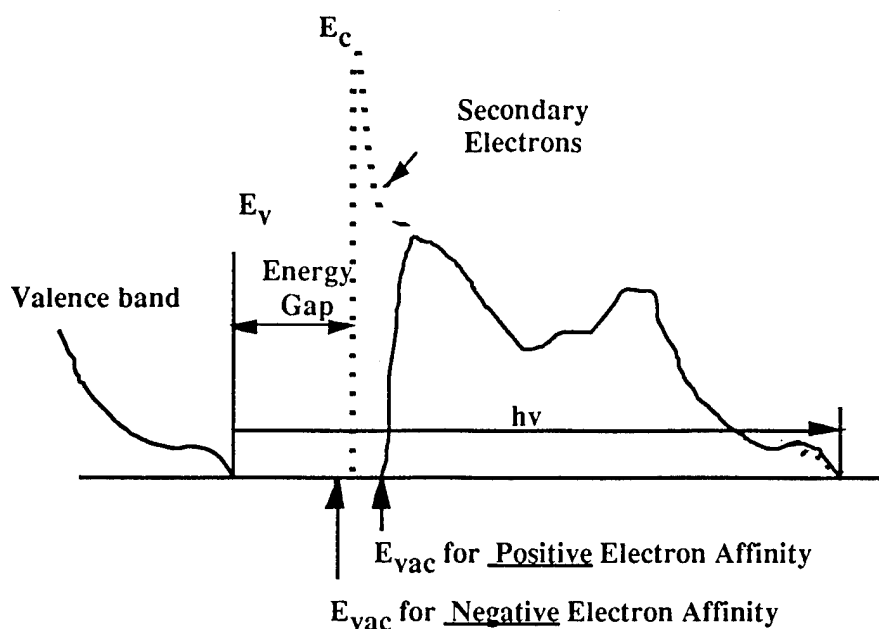
Figure 2.   A schematic of the difference in the photoemission spectra of a semiconductor with a positive or negative electron affinity.

B. Experimental Procedure

The 6H-SiC substrates used in this study were supplied by Cree Research, Inc. The samples were n-type with doping concentrations of 10^{16} to $10^{18}/cm^3$. The AlGaN samples were grown by CVD in a remote location and transported in ambient to the analysis system. To avoid surface contamination, AlN and GaN samples were also grown in the integrated UHV transfer system by gas source molecular beam epitaxy (GSMBE). This system includes the UPS system, LEED, Auger, hydrogen and argon plasma processing chamber, and XPS as well as the GSMBE. The system is described elsewhere [9,11]. Recently added is the capability of GSMBE to grow undoped AlN and GaN films.

The AlGaN thin films were grown on vicinal n-type, Si-face $\alpha(6H)$-SiC(0001) substrates at 1100°C. Vicinal wafers were SiC(0001) 3°-4° off-axis toward the <11$\overline{2}$0>. The as-received SiC wafers were cut into 7.1 mm squares. The SiC pieces were degreased, dipped into a 10% HF solution for 10 minutes to remove the thermally grown oxide layer and blown dry with N_2 before being loaded onto the SiC-coated graphite susceptor. The reactor was evacuated to less than 3×10^{-5} Torr prior to initiating growth. The continuously rotating susceptor was RF inductively heated to the AlGaN deposition temperature of 1100°C in 3 SLM of flowing H_2 diluent. Hydrogen was also used as the carrier gas for the various metalorganic precursors. Once this growth temperature was reached and stabilized, AlGaN deposition was started by flowing triethylaluminum (TEA), triethylgallium (TEG) and ammonia (NH_3) into the reactor at 23.6 µmol/min, 10.5 µmol/min and 1.5 SLM, respectively. The approximate solid solution

alloy concentration using these growth parameters was estimated to be $Al_{0.55}Ga_{0.45}N$ from cathodoluminescence measurements. The AlGaN films were doped with Si from a SiH_4 source (8.2 ppm in N_2 balance) at flow rates between 2.89 and 5 nmol/min to minimize charging problems. The system pressure during AlGaN growth was 45 Torr. The AlGaN layer was grown for 90 minutes resulting in an approximate thickness of 1.5 μm. AlGaN samples were transported in air to the analysis system. Film concentrations were determined from the bandgap values of cathodoluminescence. Auger electron spectroscopy was also used to characterize the surface.

The GaN growth took place in a GSMBE. The cleaning procedure is similar to the above described process but differs in that once in vacuum, the substrate is annealed in a silane flux [12]. The GaN samples were not intentionally doped but since very thin films were employed, charging problems were avoided.

The UPS measurements were excited with 21.21 eV radiation (He I resonance line), and emitted electrons are collected with a hemispherical energy analyzer. The base pressure of the UPS system is 2×10^{-10} Torr and operating conditions involve pressures up to 1×10^{-9} Torr, but the higher pressure is due to the helium inflow and does not contaminate the sample. The 50 mm mean radius hemispherical electron analyzer was operated at a 0.15 eV energy resolution and a 2° angular resolution. The analyzer (VSW HA50) is mounted on a double goniometer and can be tilted with respect to the sample in two independent directions. The samples were fastened with tantalum wire to a molybdenum sample holder. The sample holder is biased by up to 3 V to allow low energy electrons to overcome the work function of the analyzer. The Fermi level of the system (sample and analyzer) is determined by UPS measurement of the sample holder with no sample bias (i.e., grounded). The sample holder can be heated to 1150 °C, and the temperature is measured by a thermocouple.

C. Results and Discussion

The UV photoemission spectra of all four samples studied here are shown in Fig. 3. The AlN and GaN films were prepared by GSMBE and transferred under UHV to the photoemission system. The two alloy samples were prepared by CVD and suffered ambient exposure. Samples were biased with 2-3 V to overcome the work function of the analyzer, and all spectra were shifted to be aligned at the valence band maximum. The spectra were scaled such that the strongest emission was the same for all curves.

The first aspect to be noted is that the spectra of the 50% aluminum alloy and AlN exhibit sharp strong features at the highest binding energy, which corresponds to the lowest kinetic energy. These features are possibly indicative of a negative electron affinity. As noted in the introduction, the feature is attributed to emission from electrons quasi-thermalized to the

conduction band minimum. The emission from the $Al_{0.13}Ga_{0.87}N$ sample is significantly weaker, and the GaN emission does not show the sharp peak at all.

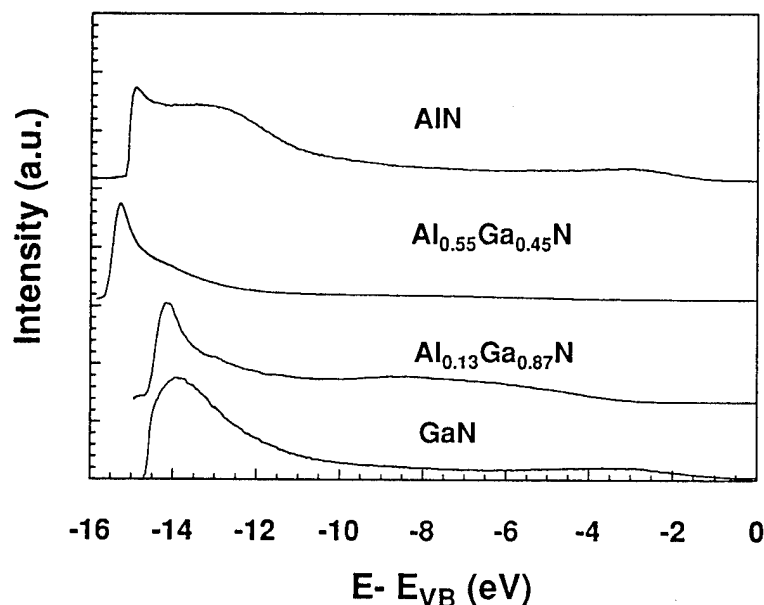Figure 3.   The UV photoemission spectra of $Al_xGa_{1-x}N$ for x=0, 0.13, 0.55, 1. Spectra were aligned at the valence band maximum.

A second indication of the change in electron affinity with alloy concentration is the extension of the $Al_xGa_{1-x}N$ spectra to lower energy as x is decreased. A more precise description of the relation of the NEA is obtained from the spectral width. The spectral width is obtained from a linear extrapolation of the emission onset edge to zero intensity at both the low kinetic energy cutoff and at the high kinetic energy end (reflecting the valence band maximum). For a material with a positive electron affinity, Fig. 2 shows that χ = hv -E_g -W, and for a material with a NEA, Fig. 2 indicates that 0 = hv -E_g -W, or rewriting, hv = E_g + W. This analysis indicates that the 50% aluminum sample does not have a negative affinity but rather a low positive affinity value, as discussed below. We note that the photoemission measurements cannot be used to determine the energy position of the electron affinity for the NEA case.

To determine the energy position of the valence band maximum, the spectral gain was increased, and the intensity was extrapolated to 0 emission. The spectra are aligned in Fig. 3 at the deduced valence band maximum. The spectral widths obtained from the $Al_xGa_{1-x}N$ samples were 14.5, 14.5, 15.5, and 15 eV for x=0, 0.13, 0.55, and 1.0, respectively. In applying the relations noted above, the bandgaps of the bulk AlN and GaN must also be known. The literature values of the AlN and GaN bandgaps are 6.2 and 3.4 eV, respectively. Assuming a linear extrapolation for the bandgap of the alloys, we deduce x=0.55 for

E_g = 4.70 eV and x=0.13 for E_g = 3.80 eV. Using the relations described above, the AlN surface satisfies the relations for a NEA within ±0.2 eV, while the GaN, $Al_{0.55}Ga_{0.45}N$, and the $Al_{0.13}Ga_{0.87}N$ surfaces do not satisfy the relations for a NEA. We can, however, determine the value of the electron affinity of these materials and find that χ = 3.3 eV, 2.9 eV, and 1.0 eV for x = 0, 0.13, and 0.55, respectively.

Another aspect that is evident from the photoemission spectra is the position of the surface Fermi level relative to the valence band maximum. It was found that E_F ranges from 2 to 3.5 eV above the valence band maximum for each sample. For the GaN and $Al_{0.13}Ga_{0.87}N$ surfaces, these values position E_F in the upper part of the gap while for the AlN (deleted rich) and 50 % Al samples, the values indicate that the surface Fermi level is pinned near midgap. The pinning at midgap may be an indication of increased impurity incorporation. In particular, the strong affinity of Al with oxygen often results in increased oxygen incorporation for these films.

To further explore the surface affinity, the effect of annealing in vacuum was explored for the x=0.55 sample. The results are shown in Fig. 4. After annealing to 475 °C and 580 °C for 10 minutes, the photoemission spectra showed a decrease in the relative intensity of the NEA related peak. Furthermore, the width of the spectra also decreases. As these temperatures are much less than the temperatures involved in growth, it is unlikely that a component present during growth is removed. It is possible that some type of contamination was introduced which
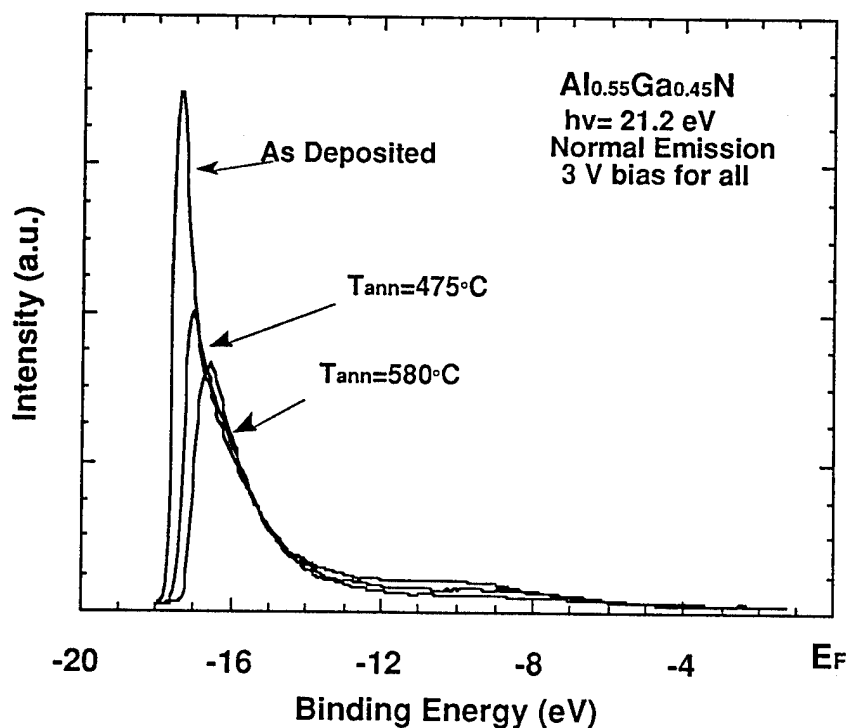

Figure 4.   The UV-photoemission from $Al_{.55}Ga_{.45}N$ on 6H-SiC versus annealing temperature.

27

affected the emission. It is suggested that hydrocarbon contaminants are a likely possibility. No LEED pattern was visible for the $Al_{0.55}Ga_{0.45}N$ sample and the lack of a LEED pattern for the as-loaded samples is possibly related to carbon and oxygen on the surface (attributed to the transport in air). The annealing may result in more complete bonding of the surface adsorbed hydrocarbon layer which results in a change in the surface dipole. Another possibility is that the electron affinity has been affected by adsorbed molecules such as hydrogen. While previous results have shown that hydrogen can induce a NEA surface on diamond [7,10], the AlGaN surfaces have not been intentionally exposed to H. It is evident that further studies are necessary to characterize the surfaces more completely.

The deduced electron affinities versus alloy concentration are shown in Fig. 5. Again, it is noted that the photoemission measurements cannot be used to determine the position of the vacuum level for a NEA surface; this point is indicated at $\chi = 0$ with an arrow to larger negative values. The results suggest that the electron affinity depends on the alloy concentration as originally suggested. Unfortunately, sufficient data is not present at this time to more completely describe the effect. Additionally, no effort to control the surface termination for these samples has been made. For diamond, it was found that the observation of a NEA is critically dependent on the surface termination. Future studies will explore whether the electron affinity of AlGaN materials is also affected by different surface preparations.
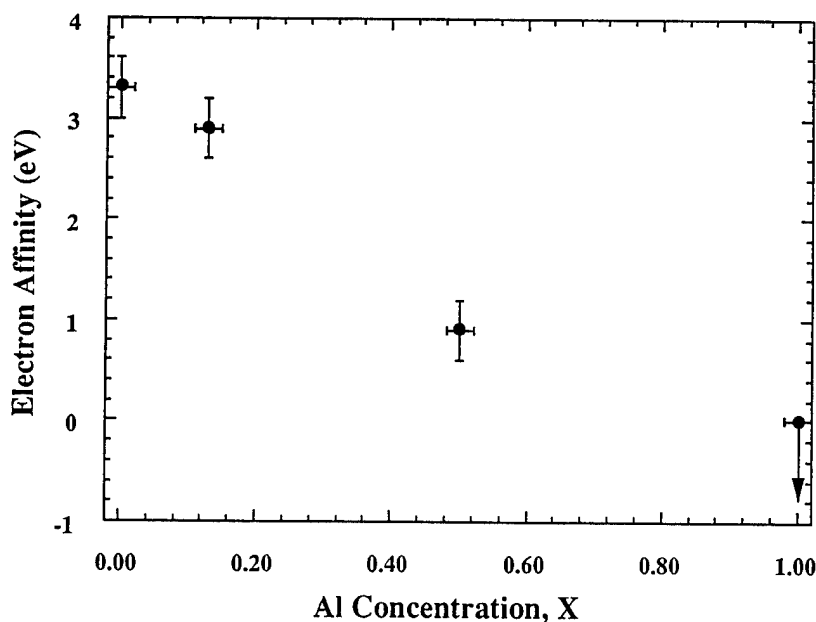

Figure 5.   Electron affinities of $Al_xGa_{1-x}N$ alloys vs. Al concentration. The arrow indicates that the electron affinity is less than (or equal) 0, but the value cannot be determined from the UV photoemission measurements.

D. Conclusions

In summary, features in the UPS spectra indicative of a NEA surface on AlN and a low positive electron affinity for $Al_{0.55}Ga_{0.45}N$ have been observed. The AlN spectra exhibited both the sharp features at low kinetic energy that have been found to be characteristic of a NEA; the width of the spectra was also consistent with the observed effect. The UPS spectra of AlGaN alloys did not show a NEA, but the measurements have been used to determine the electron affinity of GaN, $Al_{0.13}Ga_{0.87}N$, and $Al_{0.55}Ga_{0.45}N$ yielding values of 3.3, 2.9, and 01.0 eV, respectively.

The surface Fermi level was found to shift towards the middle of the bandgap for the Al-rich samples. This may indicate an increase in oxygen impurities.

The NEA surfaces were robust, showing the effect even after transfer through ambient. AlN samples grown *in situ* have shown NEA surfaces without the presence of oxygen. The positive affinity surfaces, when annealed, results in a change of the electron affinity. This effect was attributed to a change in the surface layer that affected the surface dipole.

E. Future Work

Future work will involve examining samples to fill in the gaps in the solid solution of AlGaN alloys. Furthermore, whether surface treatments can be employed on the AlGaN alloys to form stable NEA surfaces will be explored. Band offsets will be determined for GaN grown on SiC substrates.

F. Acknowledgments

G. References

1. S. Strite and H. Morkoç, J. Vac. Sci. Technol. B **10** 1237 (1992).
2. J. H. Edgar, J. Mater. Res., 7, 235 (1992).
3. M. D. Williams, M. D. Feuer, S. C. Shunk, N. J. Sauer, and T. Y. Chang, J. Appl. Phys. **71**, 3042 (1992).
4. M. C. Benjamin, C. Wang, R. F. Davis, R. J. Nemanich, Appl. Phys. Lett. **64**, (1994).
5. M. C. Benjamin, C. Wang, R. S. Kern, R. F. Davis, R. J. Nemanich, Mat. Res. Soc. Symp. **339**, 81 (1994).
6. F.J. Himpsel, J.A. Knapp, J.A. van Vechten and D.E. Eastman, Phys. Rev. B **20**, 624 (1979).
7. B. B. Pate, Surf. Sci. **165**, 83 (1986).
8. B. B. Pate, M. H. Hecht, C. Binns, I. Lindau and W.E. Spicer, J. Vac. Sci. Technol. **21**, 364 (1982).
9. J. van der Weide and R. J. Nemanich, J. Vac. Sci. Technol. B **10**, 1940 (1992).
10. J. van der Weide and R. J. Nemanich, Appl. Phys. Lett. **62**, 1878 (1993).
11. J. van der Weide and R. J. Nemanich, Phys. Rev. B15 49 13629 (1994).
12. R. Kaplan, Surface Science **215**, 111 (1989).

V. Fabrication and Characterization of Al/AlN/SiC MIS Diodes Grown by Gas-source Molecular Beam Epitaxy

A. Introduction

Silicon carbide (SiC) is a wide bandgap material that is attractive for the fabrication of electronic devices that operate in a variety of harsh environments. Silicon carbide has a wide bandgap (≈ 3.0 eV at room temperature), excellent thermal stability [1-3], a high thermal conductivity (4.9 W cm^{-1}K^{-1}) [4], a high breakdown field (2×10^6 V cm^{-1}) [2] and a high saturated electron drift velocity (2×0^7 cm s^{-1}) [3]. In the last few years, blue light emitting diodes (LEDs), junction field effect transistors (JFETs) and metal-oxide-semiconductor field effect transistors (MOSFETs) have become commercially available. Excellent reviews of these devices have been published [5-11].

Since metal-insulator-semiconductors (MIS) structures are an important part of today's microelectronics industry, MIS diodes (using SiO$_2$, in particular, as the insulator) have been studied by a number of researchers. The majority of the studies have been done on 6H-SiC substrates. Although some work [12-16] has also been done on 3C-SiC, the defective nature of the material makes most of the measurements difficult to interpret since the resulting interface state densities and fixed oxide charge densities are very high. Most of this work has centered around the optimization of the oxidation both kinetically and electrically; however, the chemical character of the oxide has also been studied by Auger electron spectroscopy [17, 18] and secondary ion mass spectroscopy [16, 19, 20]. Nearly all reports (see, for example, [21]) show that the MOS diodes can be easily accumulated and depleted at room temperature; however, inversion cannot be obtained using typical testing procedures. The lowest reported values of fixed charge densities and interface state densities are 3×10^{11} cm^{-2} and 1.5×10^{11} cm^{-2} eV^{-1}, respectively. To date, there has only been one report [23] of a MIS diode made with an insulator other than SiO$_2$. In this case, Si$_3$N$_4$ was used, but had only minimal success due to very large density of defects and large leakage currents.

Aluminum nitride possesses a direct bandgap of 6.28 eV at 300 K [24], a melting point in excess of 2275 K [25], a thermal conductivity of 3.2 W cm^{-1} K^{-1} [26] and a low dielectric constant ($K_{AlN} = 8.5 \pm 0.2$) [27]. As such, it is a candidate material for high-power and high-temperature microelectronic and optoelectronic applications with the latter employment being particularly important in the ultraviolet region of the spectrum [24]. These properties strongly indicate that superior surface acoustic wave devices, operational in aggressive media and under extreme conditions both as sensors for high temperatures and pressures and as acousto-optic devices, can be developed [28-30]. However, progress regarding these (and other) applications is hampered by the lack of high-quality single crystal material.

Because of its thermal stability and wide bandgap, AlN has been investigated as a potential insulating material for Si [31-36], GaAs [35, 37-41] and InP [41, 42] based electronic device structures. Although Stevens *et al.* [43] have fabricated an operational Si-MISFET using AlN as the gate, only moderate success has been accomplished using AlN gates due to difficulties in growing high-quality films on these substrates. The purpose of this work was to study the feasibility of forming MISFET devices in SiC using AlN as the gate dielectric.

B. Experimental Procedure

Thin, epitaxial films of several thicknesses of AlN were grown on n-type ($N_D-N_A \approx 4\times10^{16}$ cm^{-3}) Si-face α(6H)-SiC(0001) substrates supplied by Cree Research, Inc. Each of the wafers contained a 0.8 µm epitaxial SiC layer deposited via CVD and a thermally oxidized 75 nm layer to aid in wafer cleaning. The surfaces were prepared by a 10% HF dip and a 10 minute anneal at 1050 °C in UHV, as well as a silane exposure and boil-off described in previous reports.

All growth experiments were carried out in the GSMBE system detailed in previous reports. Films of AlN were grown at 1100 °C. Source were aluminum (99.9999% purity), evaporated from a standard MBE effusion cell operated in all cases at 1150°C, and 7.0 sccm ammonia (99.999% pure). Typical base pressures of 10^{-9} Torr were used. Aluminum contacts (area = 4.558×10^{-3} cm^2) were deposited on the AlN by means of a standard evaporator and In-Sn solder was used as a backside contact to the SiC.

High frequency capacitance-voltage measurements were performed on samples $\approx$1000 Å thick using a HP 4284A LCR meter operating at 1 MHz. Samples could be tested in the dark and under illumination by a halogen lamp at temperatures up to 300 °C. The typical measurement sequence involved illuminating the sample while it is biased under depletion conditions until a stable capacitance is reached, switching the light off, sweeping the voltage from depletion into accumulation and sweeping from accumulation back to depletion. From the C-V curve and the knowledge of a few physical constants, several important parameters can be calculated.

From the C-V curve , the flat band voltage, V_{FB}, can be determined from the flat band capacitance, C_{FB}. The flat band capacitance is calculated by

$$C_{FB} = \frac{K_{AlN}\varepsilon_0}{d_{AlN} + \left(\frac{K_{AlN}}{K_{SiC}}\right)L_D} \tag{1}$$

where K_{AlN} ($\approx$9) and K_{SiC} ($\approx$10) are the dielectric constants of AlN and SiC, ε_0 is the permittivity of free space, d_{AlN} is the AlN thickness and L_D is the extrinsic Debye length in SiC. The Debye length can be calculated according to the relation

31

$$L_D^{SiC} = \sqrt{\frac{K_{SiC}\varepsilon_0 kT}{Nq^2}} \qquad (2)$$

where k is Boltzmann's constant, T is temperature, N is the doping level in the SiC and q is the carrier charge.

Having determined the flat band capacitance, the flat band voltage can be read directly from the C-V curve. The deviation of this number from ideality (determined by the difference in the work functions of the Al metal and the SiC) can, in turn, be used to determine the interface charge trap density per unit area, N_t, which takes into account the density of interface states over the entire energy range of the bandgap. This density of interface charge traps can be calculated by

$$N_t = \frac{C_{AlN}^{max}}{qA}(V_{FB} - \phi_{ms}) \qquad (3)$$

where C_{AlN}^{max} is the maximum capacitance of the AlN (read from the C-V curve), A is the contact area and ϕ_{ms} is the difference in the work functions of the metal (Al) and the semiconductor (SiC). Since the value of ϕ_{Al} is 4.28 V [44] and the value of ϕ_{SiC} is 4.5 V [45], ϕ_{ms} has a value of 0.22 V.

Another interesting consequence of these measurements is the ability to determine experimentally the value of the AlN dielectric constant. Knowing the thickness of the insulator, determined by HRTEM, profilometry, SEM or some other method, the AlN dielectric constant can be calculated by the following relation

$$K_{AlN} = \frac{d_{AlN}C_{AlN}^{max}}{\varepsilon_0 A} . \qquad (4)$$

C. Results

In all cases, the diodes could be accumulated and depleted with the application of small gate voltages. However, deep depletion and inversion were not achieved in any case. Figure 1 shows a C-V curve for a typical 1000 Å sample measured at room temperature. In this particular case, where $N_D - N_A \approx 4 \times 10^{16}$ cm^{-3}, the Debye length can be calculated from Eq. 2 to be ≈ 190 Å.

Using the known data and others determined the from the graph, several other important points can be gleaned. First of all, the flat band capacitance and voltage are 310 pF and 0.7 V, respectively. Since only 0.22 V can be accounted for by the difference in the work functions of the metal (Al) and the semiconductor (SiC), the theoretical shift from flat band voltage is 0.48 V. Using Eq. 3, this translates to a density of (negatively charged) interface charge traps

of $\approx 2\times10^{11}$ cm^{-2}. From Eq. 4, the dielectric constant for AlN can be calculated to be 8.67 which fits other measured data [27] for AlN.
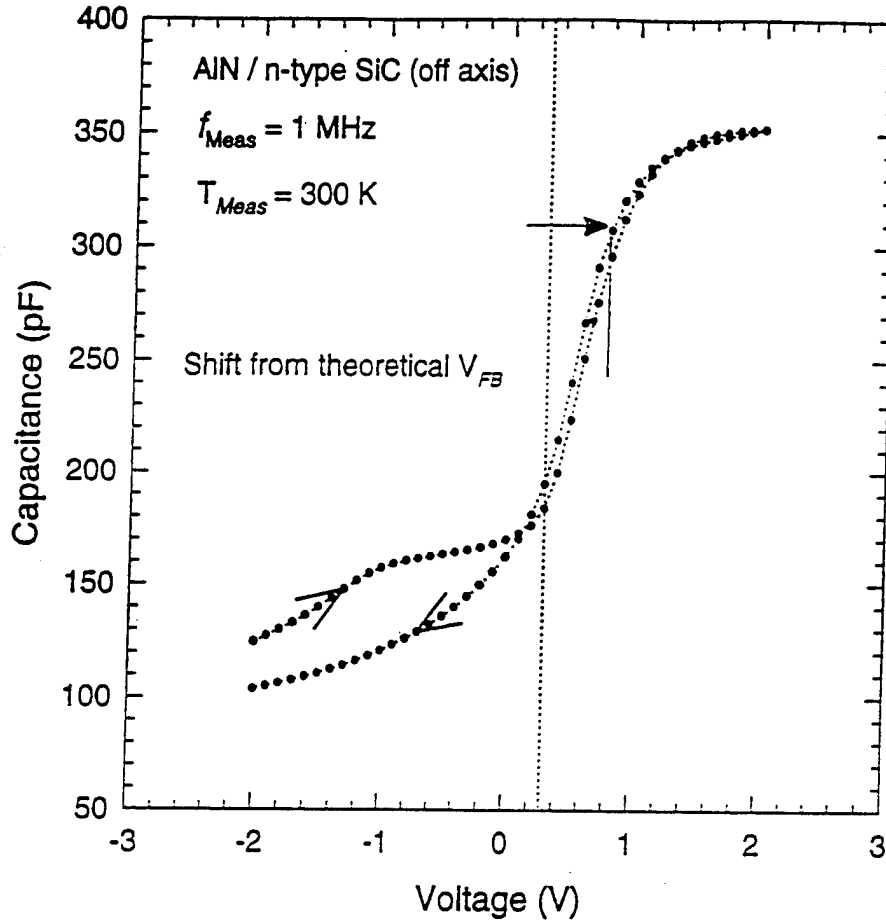

Figure 1.   Room temperature C-V measurement of an Al/AlN/SiC MIS diode.

Figure 2 shows the side-by-side comparison of the same sample swept over the voltage range at room temperature while in the dark and while under illumination. The most significant features of this figure are the shift in the flat band voltage and the increased hysteresis observed under illumination.

Figure 3 displays the effect that temperature plays on the C-V measurements. The broadening of the curve (i.e., the hysteresis) is shown to occur with increasing temperature. In contrast to the effect shown by SiO$_2$/SiC interfaces, the flat band voltage shift *decreases* in the case of AlN insulators. As a result of this effect, the net interface trap density appears to be reduced as the temperature of the measurement is made.
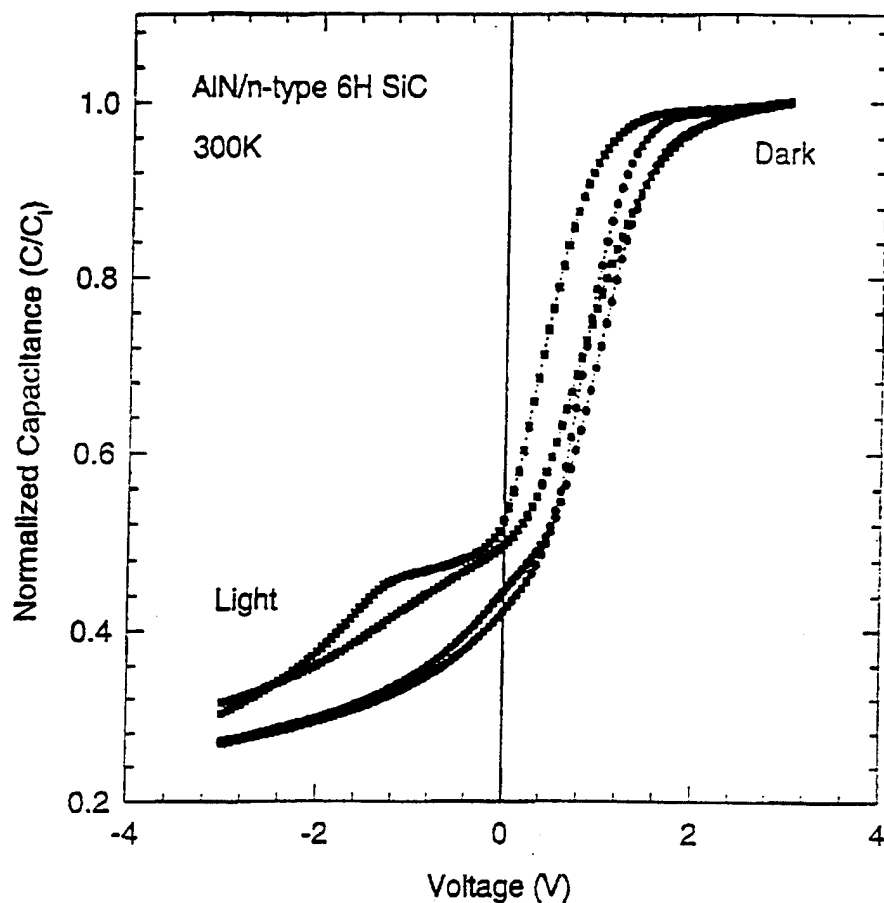
Figure 2. Room temperature C-V measurements of an Al/AlN/SiC MIS diode measured with and without illumination.

D. Discussion

Figure 1 shows the accumulation and depletion of a typical Al/AlN/SiC diode. Attempts to invert these samples at room temperature were unsuccessful. This is due to several factors. The extremely low intrinsic carrier concentration in SiC ($\approx 10^{-6}$ cm^{-3}) and the low carrier generation significantly reduce the number of minority carriers available in the SiC surface region. The low interface charge trap density and the very small amount of hysteresis make this insulator comparable to any reported thermally grown oxide layer. This curve is very similar to those done on SiO$_2$/Si MIS structures at very low temperatures (≈ 150 K) which indicates that the traps present in this interface are very slow to react to the voltage and the frequency shift. In this case, the most likely origin of the traps is unsaturated bonds at the interface and, perhaps, a slight amount of intermixing at the interface creating a number of unsatisfied bonds. Since the interface is made up of a nonisovalent bonding configuration made up primarily of Si^{+4} and N^{-3} atoms which create a net positive charge in the vicinity of the interface, the interface traps are negatively charged in order to maintain charge neutrality.
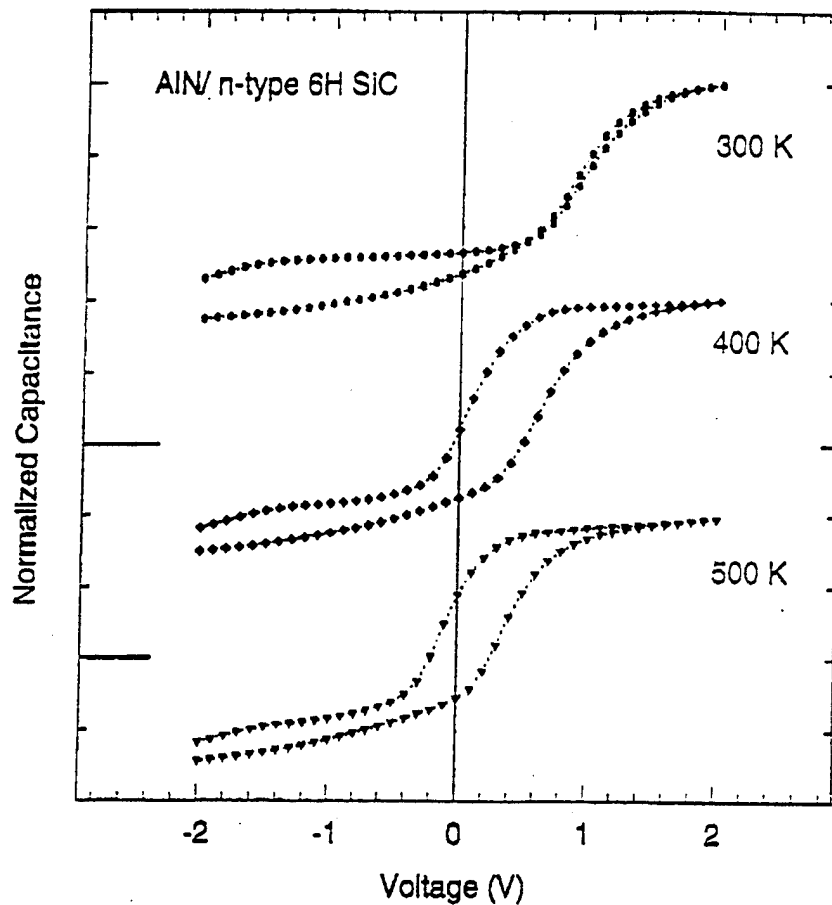
34

Figure 3.   Temperature dependence of C-V measurements of an Al/AlN/SiC MIS diode.

The effects shown in Figs. 2 and 3 are particularly interesting in their relationship to the device physics associated with the AlN/SiC interface. Figure 2 shows that the charge contained in the traps can be modulated by the application of light. Though these traps are very slow when considering only a voltage bias, their electron population can be reduced and increased by the application and removal of light. Figure 3 shows the competition between the negatively charged (acceptor-like) traps and a donor-like trap of unknown origin. At higher temperatures, the latter trap begins to control the shift in V_{FB} and pushes it to smaller values. At this point, the nature of these traps is unknown, but is speculated to be associated with the relatively high level ($\approx 10^{20}$ cm^{-3}) of oxygen tied up at the interface of the AlN layer.

E.   Conclusions

Thin AlN insulating layers on SiC have been used in MIS diode structures. The resulting diodes can be accumulated and depleted but cannot be inverted by high frequency C-V characterization. Layers thinner than 1000 Å are too leaky to measure, but 1000 Å thick layers

35

are sufficient. Very low interface trap densities ($\approx 2\times10^{11}$ cm^{-2}) and very accurate dielectric constant (8.67) values have been determined. The role of illumination and temperature have also been studied.

F. Future Research Plans and Goals

Growth will be attempted on other SiC orientations to attempt to further low the interface trap density. Passivating layers will also be deposited on the AlN to help reduce leakage currents and prevent oxidation of the material. Other attempts to reduce the impurity content are also underway.

E. References

1. R. B. Campbell and H.-C. Chang, in *Semiconductors and Semimetals, Vol. 7B*, edited by R. K. Willardson and A. C. Beer (Academic Press, New York, 1971), p. 625.
2. W. von Muench and I. Pfaffeneder, J. Appl. Phys. **48**, 4831 (1977).
3. W. von Muench and E. Pettenpaul, J. Appl. Phys. **48**, 4823 (1977).
4. G. A. Slack, J. Appl. Phys. **35**, 3460 (1964).
5. R. F. Davis, J. W. Palmour and J. A. Edmond, Mater. Res. Soc. Symp. Proc. **162**, 463 (1990).
6. R. F. Davis, in *The Physics and Chemistry of Carbides; Nitrides and Borides*, edited by R. Freer (Kluwar Academic Publishers, The Netherlands, 1990), p. 589.
7. R. F. Davis, G. Kelner, M. Shur, J. W. Palmour and J. A. Edmond, Proc. IEEE **79**, 677 (1991).
8. R. F. Davis, J. W. Palmour and J. A. Edmond, Diam. Rel. Mater. **1**, 109 (1992).
9. R. F. Davis, Phys. B **185**, 1 (1993).
10. P. A. Ivanov and V. E. Chelnokov, Semicond. Sci. Technol. **7**, 863 (1992).
11. J. A. Powell, P. G. Neudeck, L. G. Matus and J. B. Petit, Mater. Res. Soc. Symp. Proc. **242**, 495 (1992).
12. K. Shibahara, S. Nishino and H. Matsunami, Jpn. J. Appl. Phys. **23**, L862 (1984).
13. R. E. Avila, J. J. Kopanski and C. D. Fung, Appl. Phys. Lett. **49**, 334 (1986).
14. S. M. Tang, W. B. Berry, R. Kwor, M. V. Zeller and L. G. Matus, J. Electrochem. Soc. **137**, 221 (1990).
15. M. Shinohara, M. Yamanaka, S. Misawa, H. Okumura and S. Yoshida, Jpn. J. Appl. Phys. **30**, 240 (1991).
16. C. Raynaud, J.-L. Autran, J.-B. Briot, B. Balland, N. Bécourt and C. Jaussaud, J. Electrochem. Soc. **142**, 282 (1995).
17. R. W. Kee, K. M. Geib, C. W. Wilmsen and D. K. Ferry, J. Vac. Sci. Technol. **15**, 1520 (1978).
18. R. Berjoan, J. Rodriguez and F. Sibieude, Surf. Sci. **271**, 237 (1992).
19. C. Raynaud, J.-L. Autran, B. Balland, G. Guillot, C. Jaussaud and T. Billon, J. Appl. Phys. **76**, 993 (1994).
20. C. Raynaud, J.-L. Autran, F. Seigneur, C. Jaussaud, T. Billon, G. Guillot and B. Balland, J. Phys. III **4**, 937 (1994).
21. A. Rys, N. Singh and M. Cameron, J. Electrochem. Soc. **142**, 1318 (1995).
22. J. N. Shenoy, G. L. Chindalore, M. R. Melloch, J. A. Cooper, Jr., J. W. Palmour and K. G. Irvine, J. Electron. Mater. **24**, 303 (1995).
23. G. E. Morgan, C. C. Tin, J. R. Williams and R. Ramesham, in *Silicon Carbide and Related Materials*, edited by M. G. Spencer, R. P. Devaty, J. A. Edmond, M. A. Khan, R. Kaplan, and M. Rahman (Institute of Physics, Bristol, 1994), p. 645.
24. W. M. Yim, E. J. Stofko, P. J. Zanzucchi, J. I. Pankove, M. Ettenberg and S. L. Gilbert, J. Appl. Phys. **44**, 292 (1973).

25. M. G. Norton, P. G. Kotula and C. B. Carter, J. Appl. Phys. **70**, 2871 (1991).
26. G. A. Slack, J. Phys. Chem. Solids **34**, 321 (1973).
27. S. Strite and H. Morkoc, J. Vac. Sci. Technol. B **10**, 1237 (1992).
28. J. K. Liu, K. M. Lakin and K. L. Wang, J. Appl. Phys. **46**, 3703 (1975).
29. M. Morita, N. Uesugi, S. Isogai, K. Tsubouchi and N. Mikoshiba, Jpn. J. Appl. Phys. **20**, 17 (1981).
30. G. D. O'Clock, Jr. and M. T. Duffy, Appl. Phys. Lett. **23**, 55 (1973).
31. S. Mirsh and H. Reimer, Phys. Stat. Sol. **11**, 631 (1972).
32. J. Bauer, L. Biste, D. Bolze and G. Eichorn, Phys. Stat. Sol. **399**, 173 (1977).
33. M. Morita, S. Isogai, K. Tsubouchi and N. Mikoshiba, Appl. Phys. Lett. **38**, 50 (1981).
34. M. Morita, K. Tsubouchi and N. Mikoshiba, Jpn. J. Appl. Phys. **21**, 728 (1982).
35. M. Koshinaka, H. Fujii, K. Nakanishi and Y. Shibuya, Vacuum **41**, 1971 (1990).
36. A. U. Ahmed, A. Rys, N. Singh, J. H. Edgar and Z. J. Yu, J. Electrochem. Soc. **139**, 1146 (1992).
37. F. Alexandre, J. M. Masson, G. Post and A. Scavennec, Thin Solid Films **98**, 75 (1982).
38. S. Fujieda, J. Mizuki and Y. Matsumoto, Jpn. J. Appl. Phys. **27**, L296 (1988).
39. S. Fujieda, Y. Mochizuki, K. Akimoto, I. Hirosawa, Y. Matsumoto and J. Matsui, Jpn. J. Appl. Phys. **29**, L364 (1990).
40. Y. Mochizuki, M. Mizuta, S. Fujieda and Y. Matsumoto, J. Appl. Phys. **67**, 2466 (1990).
41. P. Bhattacharya and D. N. Bose, Jpn. J. Appl. Phys. **30**, L1750 (1991).
42. S. Fujieda, K. Akimoto, I. Hirosawa, J. Mizuki, Y. Matsumoto and J. Matsui, Jpn. J. Appl. Phys. **28**, L16 (1989).
43. K. S. Stevens, M. Kinniburgh, A. F. Schwartzman, A. Ohtani and R. Beresford, Appl. Phys. Lett. **66**, 3179 (1995).
44. R. M. Eastment and C. H. B. Mee, J. Phys. F **3**, 1378 (1973).
45. J. A. Dillon, Jr., R. E. Schlier and H. E. Farnsworth, J. Appl. Phys. **30**, 675 (1959).

VI. Distribution List

Dr. Yoon Soo Park   3
Office of Naval Research
Applied Research Division, Code 1261
800 N. Quincy Street
Arlington, VA 22217-5660

Administrative Contracting Officer   1
Office of Naval Research
Regional Office Atlanta
101 Marietta Tower, Suite 2805
101 Marietta Street
Atlanta, GA 30332-0490

Director   1
Naval Research Laboratory
ATTN: Code 2627
Washington, DC 20375

Defense Technical Information Center   2
Bldg. 5, Cameron Station
Alexandria, VA 22304-6145